Master Thesis

submitted within the UNIGIS MSc programme
at the Centre for GeoInformatics (Z_GIS)
Salzburg University

Extraction of features from an alpine rock face based on lidar data

development of new methods using the Monte Rosa east face as an example

by

Dipl. Geol. Roger Wiss
U1302

A thesis submitted in partial fulfilment of the requirements of
the degree of
Master of Science (Geographical Information Science & Systems) – MSc (GISc)

Advisors:

Dr. Ross Purves
Dipl. Natw. ETH Luzia Fischer, PhD student
Ao. Univ.-Prof. Mag. Dr. Josef Strobl

Basel, 30 June 2009

Acknowledgements

First of all I want to thank Ross Purves and Luzia Fischer from the University of Zurich for taking over the technical supervision of this study. It was Ross who suggested this compelling topic for me to work on. Both provided valuable ideas and literature, patiently answered my questions, and thoroughly reviewed and improved the manuscript.

I would also like to thank my main supervisor Josef Strobl who was always present in the background and answered quickly if questions arose. He also provided me with an important contact person. All my supervisors helped and encouraged me during the whole of the work.

I would like to thank Lucian Dragut for an interesting discussion on feature extraction and for providing me with relevant literature on the topic. Many thanks to Julien Vallet who patiently answered questions on the lidar dataset, and to Bernhard Zagel and Matthias S. Möller for their help regarding aerial image analysis. I am also thankful to Michel Jaboyedoff and Richard Metzger who were willing to support me regarding Coltop-3D.

Many thanks to all my colleagues and friends who supported me in one way or another in the successful completion of the thesis, especially to Nils, Achim, Dea, Pierre, and Kay. I would like to thank my parents and my brother who supported me all along.

Finally, I am especially grateful to Katy for her critical review of the manuscript and for fruitful discussions on the topic. I am also indebted to her for her patience and moral support during my work on this thesis.

This master thesis is related to the SNF project “Slope instabilities in perennially frozen and glacierised rock walls: analysis and modelling” (Nr. 200021-111967) and to the research project “Monte Rosa east face” (Nr. 21291) of the ETH Zurich.

Declaration of own work

I confirm that this master thesis was written without the help of others and without using any sources other than the ones cited and that this thesis has not been submitted in its present form or a similar form to another examination board. All passages in this thesis that are quoted from other sources are marked accordingly.

Basel, June 2009

Roger Wiss

Abstract

In recent decades, glacier retreat and permafrost degradation have led to increased slope instabilities, which present a major threat to the population in mountainous regions. In order to recognise potential risks, it is important to identify hazard-related objects. For areas that are large or difficult to access, automated detection and delineation of such objects has great potential.

This work investigates automated object extraction from a DEM of a steep alpine rock face, which is a new research field with particular challenges due to very steep slopes. Helicopter-borne high-resolution laser scanning elevation and intensity data of the Monte Rosa east face, Italy, one of the highest flanks in the Alps, is used as an example. Two approaches are applied: (1) recommendations on the suitability of three *specific methods* are made: classification into six morphometric classes, application of terrain roughness and of laser scanning reflectance intensity; (2) new methods for the extraction of four *specific objects* are evaluated: geological planes, steep fronts of hanging glaciers, snow and ice cover, and crevasses. Where necessary, an orthorectified aerial image (orthophoto) is used as a control or auxiliary dataset. The influence of scale on feature extraction is investigated, with all methods being applied at different scales, ranging from 1 up to 25 m grid resolution.

This study shows that geological planes can be accurately extracted using a combination of slope and aspect. Thus, individual discontinuities that extend over the whole wall can easily be identified. The approximate slope and aspect of the planes is recognisable at a glance. Six of eight existing steep fronts were identified using Canny edge detection and the orthophoto as an auxiliary dataset; one obtained edge could not be validated as a steep front. Snow and ice cover can be recognised from the DEM alone with an accuracy of approximately 70 % through the application of a terrain roughness measure. Crevasses can be recognised using Canny edge detection and the orthophoto, but they cannot be distinguished from other surface irregularities and artefacts. The classification into six morphometric classes gives a quick overview of ridge- and channel-like features, but is not suitable for the extraction of planar surfaces. The applied terrain roughness measurement method is suitable for steep faces, but edges at all scales are also seen as rough. Laser scanning intensity data was not applied for feature extraction because it is not homogeneous due to external influences during acquisition.

The influence of scale on feature extraction is significant; hence a multi-scale approach is imperative. Most features can only be identified at a specific scale or within a certain scale

range. Usually, the ideal working scale corresponds to the minimum extent of the target feature. It is not possible to assign a most suitable scale to a method if a target feature is not defined. The choice of the grid interpolation method has an influence on the outcome of feature extraction. The determined thresholds for the extraction of the snow and ice cover and the steep fronts depend on various factors such as scale and the grid interpolation method. Therefore, they cannot be blindly transferred to another study area but have to be visually examined.

Further work should improve object extraction from steep alpine rock faces by using an object-oriented approach and "real" 3D data as a basis. The extraction of more hazard-related features such as avalanche starting zones will be desirable.

Zusammenfassung

Während der letzten Jahrzehnte haben Gletscherschwund und Permafrostdegradation zu erhöhten Wandinstabilitäten geführt, die eine zunehmende Bedrohung in besiedelten Gebieten darstellen. Um potentielle Risiken zu erkennen, ist es wichtig, gefahrenbezogene Objekte identifizieren zu können. Bei grossflächigen und schwer zugänglichen Gebieten birgt die automatische Extraktion solcher Objekte ein grosses Potential.

Diese Arbeit untersucht die automatische Objekt-Erkennung aus einem digitalen Höhenmodell (DHM) einer steilen alpinen Felswand. Es handelt sich dabei um ein junges Forschungsfeld, mit besonderen Herausforderungen angesichts der starken Neigung. Mit dem Hubschrauber erhobene, hochauflösende Laserscanning-Daten mit Höhen- und Intensitätswerten der Monte-Rosa-Ostwand, Italien, einer der höchsten Steilwände der Alpen, werden als Beispiel verwendet. Zwei verschiedene Ansätze werden untersucht: (1) Empfehlungen zur Eignung dreier *spezifischer Methoden* werden ausgesprochen: Klassifizierung in sechs morphometrische Klassen, Anwendung der Gelände-Rauigkeit sowie der Intensitätswerte der Laserscanning-Daten; (2) neue Methoden zur Extraktion vier *spezifischer Objektarten* werden evaluiert: geologische Flächen, steile Fronten von Hängegletschern, Schnee- und Eisbedeckung sowie Gletscherspalten. Wo nötig, wird ein orthorektifiziertes Luftbild (Orthofoto) als Kontroll- oder Zusatzdatensatz verwendet. Der Einfluss der räumlichen Auflösung (engl. *scale*) bei der Objekt-Extraktion wird untersucht, wobei alle Methoden bei verschiedenen Auflösungen, die sich über 1–25 m erstrecken, angewendet werden.

Diese Studie zeigt, dass geologische Flächen unter Verwendung einer Kombination von Steigung und Exposition (engl. *aspect*) extrahiert werden können. Dadurch können individuelle Diskontinuitäten, die sich über die gesamte Wand erstrecken, auf einfache Weise identifiziert werden. Die ungefähre Steigung und Exposition der Flächen ist auf einen Blick ablesbar. Sechs von acht existierenden steilen Fronten konnten unter der Verwendung des Kanten-Detektions-Verfahren von Canny und des Orthofotos als Zusatzdatensatz identifiziert werden; eine der so erhaltenen Kanten konnte nicht als steile Front bestätigt werden. Die Schnee- und Eisbedeckung kann vom DHM mit einer Genauigkeit von ungefähr 70 % unter Anwendung der Gelände-Rauigkeit erkannt werden. Gletscherspalten können wie die steilen Fronten unter Verwendung der Canny-Kanten-Detektion und des Orthofotos identifiziert werden. Sie können jedoch nicht von anderen Oberflächen-Unregelmässigkeiten und

Artefakten unterschieden werden. Die Klassifikation in sechs morphometrische Klassen erlaubt einen raschen Überblick über Grat- und Rinne-ähnliche Objekte, ist aber nicht zweckdienlich für die Extraktion ebener Flächen. Die angewendete Methode zur Messung der Oberflächen-Rauigkeit ist für Steilhänge geeignet, jedoch werden Kanten bei allen Auflösungen als rau erkannt. Die Intensitätswerte der Laserscanning-Daten wurden nicht für die Objekt-Extraktion verwendet, da sie aufgrund externer Einflüsse bei der Datenerhebung nicht homogen sind.

Der Einfluss der räumlichen Auflösung auf die Objekt-Extraktion ist signifikant. Daher ist eine Herangehensweise über mehrere Auflösungen unerlässlich. Die meisten Objekte können nur bei einer spezifischen Auflösung oder innerhalb eines bestimmten Auflösungsbereichs identifiziert werden. Für gewöhnlich entspricht die ideale Auflösung der Mindestausdehnung des Zielobjektes. Es ist nicht möglich, für eine Methode die bestgeeignete Auflösung anzugeben, wenn kein Zielobjekt definiert ist. Die Wahl der Gitter-Interpolationsmethode übt einen Einfluss auf die Objekt-Extraktion aus. Die ermittelten Schwellenwerte zur Extraktion der Schnee- und Eisbedeckung sowie der steilen Fronten hängen von mehreren Faktoren wie der räumlichen Auflösung und der Gitter-Interpolationsmethode ab. Aus diesem Grund können die Schwellenwerte nicht blind in ein anderes Studiengebiet übertragen werden, sondern müssen visuell geprüft werden.

Weiterführende Arbeiten sollten die Objekt-Extraktion von alpinen Steilhängen verbessern, indem ein Objekt-orientierter Ansatz und “echte” 3D-Daten als Basis verwendet werden. Die Extraktion weiterer gefahrenbezogener Objekte wie Anrisszonen könnte erstrebenswert sein.

Contents

List of Figures

List of Tables

1 Introduction

1.1 Motivation

In recent decades slope instabilities influenced by glacier retreat and permafrost degradation have become a growing threat to populated and touristically used mountain areas. Therefore it is becoming more and more important to foresee hazards such as rock and ice avalanches by analysing steep rock faces (e.g. Fischer et al., 2006)

The identification of hazard-related objects such as unfavourable geological structures or steep fronts of hanging glaciers is important to evaluate the instabilities and the associated potential danger. For areas that are extensive or difficult to access, automated identification and extraction of such objects can be useful (e.g. Jaboyedoff et al., 2004).

Computer-based object extraction from digital elevation models (DEMs) as well as from satellite and aerial imagery has been carried out for decades. But high-resolution data that permit the identification of fine-scale objects have only been available for a few years.

With laser scanning, also called lidar (*li*ght *d*etection *a*nd *r*anging), an efficient technology for the acquisition of DEMs is available. Recently, high-density lidar data was obtained from the Monte Rosa east face, Northern Italy, one the highest and most impressive flanks in the European Alps, which has lately been experiencing growing slope instabilities due to glacier retreat.

Although feature extraction from a DEM is relatively common, its application to steep high-alpine rock faces is a new area of research, with particular challenges due to the very high slope. Now that high-resolution lidar data of the Monte Rosa east face are available, it is possible to investigate the use and limits of feature extraction from alpine flanks. The results of this study may improve the analysis and understanding of slope instabilities, which will therefore help recognise and foresee potential danger and possibly save human lives.

1.2 Aims of the study

The main goal of this study is to develop methods for extracting features from an alpine, partially glaciated rock face using the lidar data of the Monte Rosa east face as an example. Two approaches will be applied. On the one hand, extraction of specific features that are connected to the current hazards will be attempted. On the other hand, specific methods will be evaluated with respect to their possible suitability for the analysis of steep alpine rock faces. The influence of scale in general will be considered and described.

More specifically, the study has the following objectives:

1. To find appropriate methods for the automated extraction of features from a partly glaciated rock face, with the features being relevant to on-going natural hazard processes. Such features are: (1) snow and ice cover, (2) steep fronts, (3) crevasses, and (4) geological planes.

2. To test some specified methods with respect to their suitability for characterising a partly glaciated alpine rock face. Those methods are (1) the six morphometric classes by Wood (1996), (2) the application of terrain roughness, and (3) of lidar reflectance intensity.

3. To consider and describe the influence of scale on all feature extraction methods that were evaluated within this study.

1.3 Structure of the thesis

The thesis is divided into seven chapters. Chapter two reviews the literature on feature extraction and on investigations in the Monte Rosa east face, and uncovers research gaps. In the third chapter the geology and glaciology of the study area as well as the available lidar dataset and orthophoto are reviewed. Chapter four explains the methodologies used for feature extraction. The results of the feature extraction evaluations are presented in chapter five and discussed in chapter six. The seventh chapter concludes the study by setting the results in context to the aims of the thesis and gives an outlook on possible further work.

2 Literature review

This chapter reviews the research on feature extraction from a digital elevation model (DEM) — specifically of glaciated alpine rock faces — and gives an insight into the state of research relating to the Monte Rosa east face. It concludes with those remaining research gaps that shall be addressed within this study.

2.1 The digital elevation model

The term *digital elevation model*, which is used inconsistently in literature (Weibel and Heller, 1991), is defined here in accordance with the terms of Burrough (1986) as "a gridded set of points in Cartesian space attributed with elevation values that approximate Earth's ground surface". Thus, a DEM implies that heights need to be calculable for any point in the area of interest (Hengl and Evans, 2008).

Considering their design, all DEMs can be categorised into two groups: raster-based and vector-based (or irregular) DEMs (Weibel and Heller, 1991). In this study raster-based DEMs were used for all analyses. The key advantage of gridded DEMs is that they are amenable to processing with algorithms (Evans, 1972; Hengl and Evans, 2008).

Further advantages are that simpler algorithms can be used, and that they are more adapted to computer models used in image processing (Hengl and Evans, 2008). However, there are some notable disadvantages of gridded DEMs, one of the most important being the fact that grids under-sample topography in areas where the topography is complex, and they over-sample smooth topography (Hengl and Evans, 2008).

In general there are three sources of DEM data: ground survey techniques (e.g. GPS), existing topographic maps (contours), and remote sensing (aerial photography, lidar, and radar) (Nelson et al., 2008). For the production of the DEM used within this study lidar (light detection and ranging) has been used (sec. 3.2.1). The biggest advantages of lidar are high densities of samples and high vertical accuracy (Nelson et al., 2008). A disadvantage is that the accuracy of the readings varies according to the characteristics of the terrain (Nelson et al., 2008). For example, it may be impossible to measure very steep slopes accurately

(Smith, 2005). The company Helimap System®, which obtained the lidar data of the Monte Rosa east face, circumvents this problem by oblique lidar mapping using a helicopter (e.g. Buckley et al., 2008).

2.2 Geomorphometry

Morphometry, the measurement of shape, has been used in many branches of science ranging from biology and palaeontology (Elewa, 2004, e.g.) to mathematics and image processing (Serra, 1982). In geosciences, the term geomorphometry is used for describing "the quantitative study of the shape of the Earth's surface" (Pike, 2000). An up-to-date and complete description of concepts, software, and applications in geomorphometry is contained in Hengl and Reuter (2008).

2.2.1 Geomorphometric algorithms

Most geomorphometric algorithms perform neighbourhood operations, which can be split into focal, zonal, and global (e.g Pike et al., 2008; Straumann and Purves, 2008). In focal analysis, a small, often 3x3, regular cell matrix (also known as window, filter window, sampling window or kernel) is moved over the entire grid whereby a mathematical formula is repeated at each cell (Pike et al., 2008). Typical parameters obtained are first-order (slope angle and slope aspect[1]) and second-order derivatives (concavity, convexity).

In zonal analysis the calculations are performed inside defined regions, for instance in order to obtain statistical parameters such as the range of values (difference between highest and lowest value; Mark, 1975).

Global analysis is usually carried out over the whole grid, where typical applications are calculating the visibility between two cells or the distance from one cell to all other cells.

2.2.2 Land-surface parameters and objects

Whilst geomorphometry is used to denote the scientific discipline, the land surface itself is the principal object of study (Pike et al., 2008). Parameters and objects are the two DEM-derived entities fundamental to modern geomorphometry (see e.g. Mark and Smith, 2004). A land-surface parameter is a descriptive measure of surface form, e.g. slope, aspect, or curvature. In contrast, a land-surface object is a discrete spatial feature, e.g. a mountain, a peak, or a crevasse.

[1] *slope angle* and *slope aspect* are in the future referred to as *slope* and *aspect*, respectively.

Some morphometric parameters can be derived directly from a DEM without further knowledge of the area represented, hence they are sometimes referred to as basic land-surface parameters. They can be divided into two main groups: geometric and statistical measures (Olaya, 2008).

Geometric parameters

Evans (1979) considered five terrain parameters that may be defined to any two dimensional continuous surface: elevation, slope, aspect, profile convexity, and plan convexity, corresponding to groups of 0 (elevation), 1st (slope and aspect), and 2nd order differentials (profile convexity, and plan convexity). Whilst higher derivatives may also be extraxcted, there is no evidence that these have any geomorphological meaning (Wood, 1996).

Statistical parameters

Common statistical land-surface parameters are mean value, standard deviation, skewness coefficient, and the kurtosis coefficient (Olaya, 2008). Many statistical parameters overlap with geometric parameters, for example, standard deviation, which is strongly correlated with slope (Olaya, 2008). Other interesting statistical measures are range of values, elevation-relief index, or ruggedness.

Another interesting but not-so-basic statistical parameter is terrain roughness, which describes how undulating or complex the terrain is (Olaya, 2008). There is no clear agreement on how to calculate terrain roughness. The standard deviation of elevation has often been used as a measure for terrain roughness (Miliaresis and Kokkas, 2007). However, this can lead to incorrect results in smooth sloping terrain, since the terrain is seen as rough (Olaya, 2008). A better approach is to fit a plane to the cells in the neighbourhood, and then calculate the standard deviation of the plane instead (Sakude et al., 1998; Höfle et al., 2007). In contrast to the methods already described, Hobson (1972) proposed a vector approach to define the Surface Roughness Factor (SRF). Sappington et al. (2007) created a Vector Ruggedness Measure (VRM), which is based on Hobson's method.

Terrain roughness has been used in previous work in order to extract features. For instance, Höfle et al. (2007) used terrain roughness in addition to the intensity of the laser beam reflectance to identify ice, firn, snow and surface irregularities such as crevasses and superficial streams in glaciers.

2.2.3 General and specific morphometry

Evans (1972) divided geomorphometric analysis into two overarching modes: general and specific geomorphometry. General morphometry applies to the extraction of land-surface parameters and describes the continuous land surface (MacMillan and Shary, 2008; Pike et al., 2008). It provides a basis for the quantitative comparison even of qualitatively different landscapes (MacMillan and Shary, 2008). Specific morphometry applies to the extraction of discrete land-surface objects, best represented as vector elements, such as lines or polygons extracted from a gridded DEM (Pike et al., 2008). Some of the approaches were designed to identify certain features types, e.g. linear or circular forms (Cross, 1988), or specific forms, e.g. mountains (Miliaresis and Argialas, 1999), hill tops (Tribe, 1990), landslides or strike ridges (Chorowicz et al., 1995), craters and channels on Mars (Bue and Stepinski, 2006), drumlins (Evans, 1987), sand dunes and volcanos (MacMillan and Shary, 2008), watersheds, drainageways, and other breaklines (Evans et al., 2008). Not only geomorphological, but also specific glaciological objects have been extracted such as whole glaciers or crevasses (Kodde et al., 2007).

Many forms of measurement fall somewhere between the two extremes of general and specific morphometry (Wood, 1996). In general morphometry, parameterisation is relatively universal but not precise; specific geomorphometry is precise, but can only be applied in a limited context (Wood, 1996).

2.2.4 Extracting areas and lines

Usually, features of the two geometric types *area* and *line* are extracted from a DEM. The approaches vary widely.

Extracting areas

The word area has been chosen deliberately and comprises all area type elements having a (crisp or fuzzy) boundary such as regions or segments. Areas can be extracted by classification, supervised or unsupervised. Supervised classification can be used, if the classes are known but not exactly defined. In this case, training data is provided. If the classes are not known, unsupervised classification (also known as clustering) has to be used, with the determined optimal number of target classes as input (see Hengl and MacMillan, 2008, p. 450).

There have been proposed several schemes for the supervised classification of DEMs. Dikau (1989) defined classes of form elements by logical combination of derivatives of a

DEM. Wood (1996) put forward a similar scheme that divides a DEM into the six moprhometric classes ridge, plane, channel, pit, peak, and pass. This classification scheme can lead to crisp (e.g. Bolongaro-Crevenna et al., 2005) or fuzzy classes (e.g. Fisher et al., 2004). In fuzzy set theory, the membership of a pixel to a class is not boolean (1 or 0), but in general in between, thus fuzzy. For instance, *peakness* defines, how strongly a pixel represents a peak (or how strong the membership to the class peak is).

Extracting lines

Within the field of image processing, edge detection — i.e. the extraction of lines or boundaries — is a well established method to detect local variations of image intensity (Pitas, 1993). This technique has later often been used also in geomorphometry to extract edges — linear features of high gradient — from a DEM (e.g. Miliaresis and Argialas, 1999; Mason et al., 2006).

Edges can be identified using several approaches such as the most popular Sobel and Prewitt convolution kernels (Russ, 1999) or the sophisticated Canny filter (Canny, 1986), which is now widely used in edge detection (Li-chun, 2002; Zhou et al., 2008). The advantages of the Canny algorithm are high accuracy in edge positioning and distinction of weak edges and fake edges (noise; Zhou et al., 2008). Based on the theory of the Canny algorithm, Xu et al. (2006) propose an improved algorithm for edge detection.

2.2.5 The importance of scale

The word scale has acquired many meanings in the course of time (Longley et al., 2005):

1. Scale in the sense of spatial resolution or the level of spatial detail in data
2. Scale in the sense of geographic extent or scope of a project
3. Scale of a map

Within this study scale is being referred in the first sense, that is to say as the spatial resolution or the level of spatial detail.

The influence of scale on geomorphological analysis has been pointed out in many studies. Gerrard and Robinson (1971) recognised strong variation in slope measurement with different sampling intervals. Garbrecht and Martz (1994) identified an effect of DEM grid size on automated drainage network identification. “What becomes clear from these (and many other) studies, is that it is unwise to ignore the scale based effects of sampling interval when characterising surfaces” (Wood, 1996).

Cell size

In the analysis of gridded DEMs the influence of scale is particularly related to (1) the cell size of the grid and (2) the considered neighbourhood.

Cell size[2] — the distance between two grid nodes — can be closely related to the level of detail or spatial precision of a map, which, in cartography, is often related to the concept of scale (Hengl and Evans, 2008). As the cell size grows and the grid becomes coarser, the information content of the map will decrease, and vice versa.

The land-surface parameters slope, aspect, and curvature are very sensitive to cell size, with second derivatives (curvatures) more than first derivatives (slope, aspect; Shary et al., 2002). The influence of cell size on slope is a textbook example (Hengl and Reuter, 2008): if you reduce grid resolution (or increase cell size) the mean slope of a defined area decreases. As soon as the grid resolution becomes one, which means that the area consists of exactly one cell, the (mean) slope is zero.

Thus, there is no single *best* resolution at which to compute local land-surface parameters to describe and analyse terrain (Hengl, 2006).

Neighbourhood size

As mentioned above, surface parameters and objects are usually determined from a gridded DEM by using a small sampling window (e.g. 3x3) around each cell (Pike et al., 2008). However, many authors have recognised that using a fixed size window only allows features of a certain scale to be identified (Wood, 1996; Schmidt and Andrew, 2005). In addition, such neighbourhood definitions are not stable with changing data sources and increasing resolutions but change scale as well (Strobl, 2008, p. 133).

Approaches to obtain the most suitable scale

As seen above, a fixed grid resolution and neighbourhood size determines the level of detail of land-surface parameters and objects that can be extracted. Thus, in order to provide effective surface characterisation, analysis should be applied over a range of scales, by varying grid resolution or cell size (Wood, 1996; Schmidt and Andrew, 2005).

In order to obtain the most suitable scale (grid resolution or neighbourhood size) for extracting a specific parameter or object, multiple approaches have been described. Smith et al. (2006) examined the combination of grid resolutions and neighbourhood windows to suggest optimal combinations. Schmidt and Andrew (2005) presented a method to identify

[2] Cell size and grid size are often used as synonyms. They are inversely proportional to grid resolution.

dominant scale ranges of a landscape. They concluded that it is necessary to pre-process a DEM for a specific application in order to identify and delineate surface characteristics at scales relevant for the specific application.

2.2.6 Auxiliary datasets

Auxiliary datasets such as aerial photographs or satellite imagery can support the extraction of features from a DEM, e.g. for obtaining training data in supervised classification, or for evaluating the result of feature extraction obtained from a DEM. Also, reflectance intensity of the reflected laser beam in lidar has been shown to be a valuable auxiliary source for extracting features Höfle et al. (2007). Reflectance intensity values of the on-hand lidar data are available.

2.3 The Monte Rosa east face

Until now, the state of research of DEM analysis has been described. In this section the state of research relating to geology and natural hazards that have occurred in the study area, the Monte Rosa east face, are reviewed.

2.3.1 Geology and recent hazards

Bearth (1952) gave an early description of the geology of the Monte Rosa, followed by further examinations by Fischer (2006). For a few years, developing slope instability (Haeberli et al., 2002) and a drastic decrease in glaciation on the east face of the Monte Rosa have been observed, which have uncovered large rock areas (Kääb et al., 2004). Further investigations were carried out by Fischer (2006), who described the Monte Rosa east face as a current example of changes and developments concerning slope instabilities in rock and ice and enhanced gravitational mass movements such as rock falls, debris flows and ice avalanches.

2.3.2 Analysis using remote sensing data

Kääb (2008) provides an overview of remote sensing methods suitable for glacier and permafrost hazard assessment and disaster management. He found that DEMs are some of the most important data sets for investigating permafrost-related mass movements and thaw and heave processes. Combined with results from spectral image data and with multi-temporal data the detection of hazards is being significantly improved (Kääb, 2008). At present Fischer (in prep) is analysing and modelling slope instabilities in perennially frozen and glaciated rock walls using multi-temporal image and elevation data.

2.4 Extracting features from a glaciated alpine rock face

Automated feature extraction is useful when areas have to be analysed that are large or difficult to access. Multiple high-resolution lidar derived DEMs of steep alpine glaciated rock faces have been analysed to date. For instance, rock falls and avalanches of the Mont Blanc massif have been quantified (Ravanel et al., 2008; Rabatel et al., 2008). However, the extraction of specific features from faces of this type has not been extensively investigated to date.

2.4.1 Snow and ice cover

Snow cover information is very useful for mapping transportation and avalanche forecasting (Srivastava and Stroeve, 2003; Venkataraman et al., 2008). The differentiation of ice/snow and rock can also be an important base for further analysis. To date snow has been detected from satellite images (Srivastava and Stroeve, 2003; Venkataraman et al., 2008), but not solely from DEMs.

2.4.2 Steep fronts

Steep fronts are referred to as prominent steps in alpine rock faces covered by hanging glaciers. They have been recognised as the origins of potentially dangerous ice avalanches (Fischer, 2006). In order to foresee such hazards it is important to be able to identify steep fronts.

2.4.3 Crevasses

Crevasses are very common in hanging glaciers on alpine rock faces since they can compensate the high relief under glaciers (e.g. Sharp, 1988). They can indicate the velocity of the glacier flow, when multi-temporal data are being compared, hence it can be valuable to automatically detect them.

Several studies describe the extraction of crevasses from DEMs of alpine glaciers (Kodde et al., 2007; Höfle et al., 2007). For this purpose the latter used the calculated terrain roughness and the reflectance intensity of the laser scanning data. The crevasses were sometimes not detected due to snow bridges and the low point densities of a few meters (Kodde et al., 2007).

The extraction of crevasses from DEMs of hanging glaciers, which are common in alpine rock faces, has not been applied to date according to the knowledge of the author of this study.

2.4.4 Geological planes

The extraction of geological features from DEMs has been the subject of various studies. Bellian et al. (2005) conducted high-precision stratigraphic facies characterisation of outcrops. Lee et al. (2007) described an automatic linear-feature extraction algorithm for the extraction of geological lineaments.

In alpine rock faces it is of particular interest to identify bedding planes or discontinuities in order to better understand slope instabilities. In this context Derron et al. (2005) identified discontinuities by combining slope angle and slope aspect into one value, showing cells of same orientation.

2.5 Research gaps

In summary, the following research gaps shall be addressed within the scope of this thesis.

2.5.1 Specific approaches to extract features (bottom-up)

Some specific approaches for feature extraction are investigated. The term bottom-up refers to the here applied procedure to (1) define a method or parameter and (2) evaluate what can be extracted therewith and how.

The six morphometric classes by Wood (1996) He proposed a well-established method for the classification of a DEM into the six classes ridge, plane, channel, pit, peak, and pass. The method will be applied to the available DEM in order to investigate its behaviour and benefit with regard to alpine rock faces.

Terrain roughness According to the knowledge of the author terrain roughness has not been applied to alpine glaciated rock walls to date. This will be accomplished within the scope of this study, using a calculation method that is proposed to be fairly independent of slope (Sappington et al., 2007).

Lidar reflectance intensity Using lidar reflectance intensity values as an auxiliary source for feature extraction from a DEM of glacierous alpine rock faces is not yet a well established technique. Within this study it shall be investigated how useful intensity values for feature extraction from a DEM of an alpine rock face are.

2.5.2 Extraction of specific features from an alpine rock face (top-down)

The automated identification of geological/glaciological elements such as snow/ice, steep fronts, crevasses, or geological planes/discontinuities can support on-going natural hazard investigations and therefore plays a part within this study. In this context, the term top-down applies to the procedure to (1) define a specific land-surface object and (2) look for an applicable method; this procedure is converse to the one above.

Steep fronts Steep fronts play an important role in the context of natural hazards. Therefore a method shall be developed to automatically extract them from a DEM.

Crevasses Since no method seems to exist to extract crevasses from a DEM of an alpine rock face, a method shall be developed for this purpose.

Snow and ice cover To date snow cover information has not been extracted solely from a DEM. This task will be part of this study. The result will be compared to the orthophoto.

Geological planes Geological planes/discontinuities can give a good understanding of slope instabilities. A method shall be developed in order to identify the planes, which are mostly “rough” or sometimes covered by snow.

2.5.3 The influence of scale

It is widely accepted that, in order to characterise a DEM, a multi-scale approach is necessary (e.g Wood, 1996; Schmidt and Andrew, 2005). In this work, the influence of scale shall be investigated and described with respect to all specified methods and features. Eventually, the most suitable scale (or scale range) for each method or feature type should be suggested. Possibly fuzzy membership functions will be considered (Fisher et al., 2004).

3 Study area and datasets

3.1 The Monte Rosa east face

The Monte Rosa east face is located in the Valle Anzasca in Northern Italy, SW of Domodossola (45°56'N, 7°53'E, Figure 3.1). All its peaks — Signalkuppe, Zumsteinspitze, Dufourspitze and Nordend — are above 4500 m above sea level and mark the border between Switzerland and Italy (Figure 1). Featuring a height difference of 2300 m, the face is one of the highest steep faces in Europe. It has extensive ice cover and permafrost occurs over a large area (Fischer, 2006).

3.1.1 Geology and geomorphology

Based on the findings of Bearth (1952) and on the Geological Atlas of Switzerland 1:25'000, Fischer (2004) investigated and mapped the geology and geomorphology of the Monte Rosa east face. The face consists of orthogneiss and paragneiss, which belong to the penninic Monte Rosa nappe (Fischer, 2006).

The Monte Rosa east face is streaked by different joint sets, which form a complex discontinuity system (Fischer, 2006); the main jointing dips 70–85° to the NE, a further distinct set of fissures shows a similar dip (75–85°), but a direction to the ESE. This dip matches the orientation of the surfaces in the Monte Rosa east face in many places. These flanks are often cut by two further sets of fissures, with a much flatter dip.

3.1.2 Glaciology

The Monte Rosa east face is covered by hanging glaciers and névé fields (Fischer, 2006). During the last two decades significant changes have occurred. The regression of the glaciers has intensified and some névé fields have entirely melted (Fischer, 2006). Two typical features in hanging glaciers, steep fronts and crevasses, are included in the examinations within this study. Some crevasses occur within ice falls.

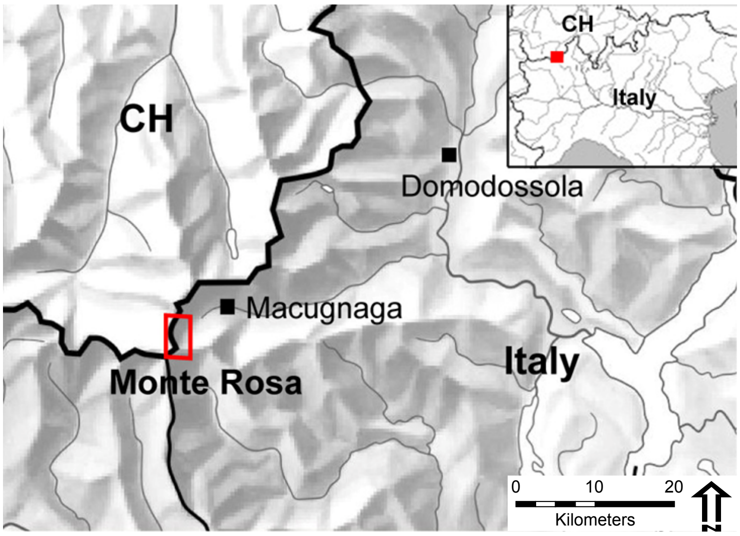

Fig. 3.1: Location of the Monte Rosa east face (red rectangle). Sketch from Fischer et al. (2006).

Fig. 3.2: Monte Rosa east face, seen from helicopter. 1 = Signalkuppe; 2 = Dufourspitze; 3 = Jägerhorn; 4 = Parete Innominata; 5 = Canalone Zapparoli; 6 = Canalone Imseng; 7 = Canalone Marinelli; 8 = Ghiacciaio del Monte Rosa. Names of objects within the face from Fischer (2006). Picture by J. Vallet (Helimap System® SA). The picture was taken on the same flight as the lidar data was obtained.

Crevasses

The most obvious, abundant, and characteristic structures of glaciers are crevasses (Sharp, 1988). A crevasse is a fracture in a glacier caused by tensile stress. Accelerations in glacier speed cause extension and can initiate a crevasse (Sharp, 1988, p. 60). The following types of crevasses occur in the Monte Rosa east face:

- *Transverse crevasses* represent the most common type and stretch across the glacier transverse to the flow direction. They clearly occur within the ice falls B, C, and D (Fig. 3.3; for a description of ice falls see below).

- *Marginal crevasses* extend diagonally from the edge of the glacier pointing up-glacier. They can be rotated by the faster central flow until they point downstream (Sharp, 1988). Marginal crevasses, for instance, are found in the middle part of the Ghiacciaio del Monte Rosa (below ice fall D, Fig. 3.3).

Ice falls

Ice fall is the term for those chaotic parts of a glacier, where the surface layer is broken into crevasses and into huge blocks called seracs due to a steep gradient and a restricted channel (Post and Lachapelle, 1971). Within this work an icefall is not seen as an ice avalanche as it is sometimes (e.g. by Pralong and Funk, 2006).

In the Monte Rosa east face four regions representing ice falls were identified (s. Fig. 3.3; L. Fischer, pers. comm.)

Steep fronts

Pralong and Funk (2006, p. 32) differentiate two types of avalanching glaciers, *terrace* and *ramp* glaciers. According to those authors, ramp glaciers are "avalanching glaciers lying on a uniform, even, steep bed"; in contrast, terrace glaciers are "avalanching glaciers with a bedrock characterized by a significant increase in slope at the glacier margin, which induces calving". This margin is referred to as steep front within this work. The discontinuity in the glacier bedrock, usually forming a rock cliff, limits the extension of the glacier which implies that ice is transferred beyond this limit and breaks off (Pralong and Funk, 2006, p. 33).

In the central part of the Monte Rosa east face eight steep fronts were identified from visual observations (Fig. 3.3, L. Fischer, pers. comm.).

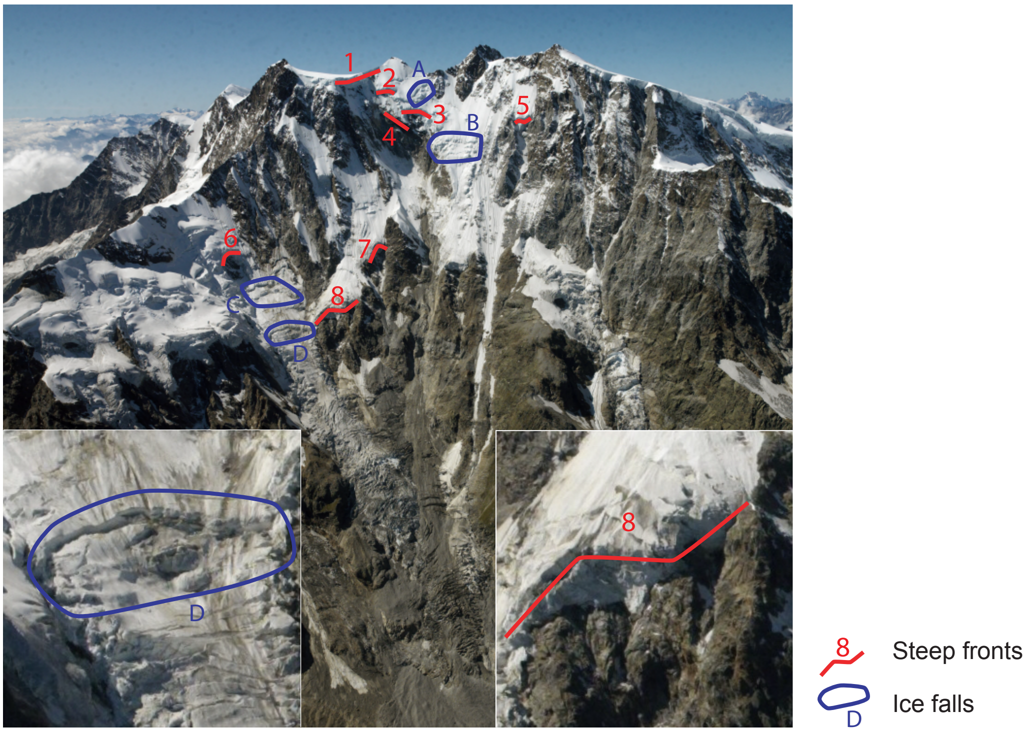

Fig. 3.3: Steep fronts and ice falls in the Monte Rosa east face (L. Fischer, pers. comm.).

3.2 Datasets

Within this study elevation data and an orthophoto, both representing the Monte Rosa east face, were used.

3.2.1 Lidar data

The available lidar data were acquired from a helicopter by the company Helimap System®SA. The Helimap system (UW+R SA; Vallet, 2007; Vallet and Skaloud, 2004) is made up of a Riegl LMS-Q240i-60 laser scanner, a digital camera and coupled GPS/INS antenna for obtaining position and orientation during data acquisition (Fischer et al., submitted). The helicopter started at the bottom of the Monte Rosa east face and flew circles upwards along the face;[1] as a result 14 horizontal flight lines were taken (Fischer et al., submitted). The data was then filtered, artefacts (birds, helicopter skids), points below surface and bad scans removed, and the fitting between the flight lines was checked (J. Vallet, pers.

[1]More details of the flight (L. Fischer, pers. comm.): date and time: September 12th 2007, 11:00–15:00; weather: fair, sunny, virtually cloudless; face partly in shadows, mainly lower part; temperature: foot of face 15 °C, peak 0–5 °C.

comm.). The point cloud consists of 4.8×10^6 points and covers an area of 3 km^2 with a point density of 1–3 pt/m^2 (Fischer et al., submitted). The horizontal position accuracy of the points amounts to less than 0.2 m (Skaloud et al., 2005). Furthermore a 1 m grid from the lidar data was provided, which had been created using an interpolation algorithm implemented in Inpho SCOP++.

The main advantage of airborne laser scanning by helicopter instead of airplane is that steep slopes look flat as the system is kept perpendicular to the terrain. In theory this reduces the occurrence of data holes through laser shadows. However, compared to another lidar dataset, which had been acquired by airplane, the helicopter lidar data reveals more data shadows (Fischer et al., submitted).

In addition to the position values x,y,z, every measurement point also includes the return amplitude or energy of the laser echo, which — in the field of airborne laser scanning — is often referred to as reflectance intensity, signal intensity or pulse reflectance of the laser signal (Höfle and Pfeifer, 2007). The reflectance intensity depends on the characteristics of the terrain surface.

3.2.2 Orthophoto

At the same time as the Monte Rosa east face was scanned, an aerial photograph was also taken from the helicopter (Fig. 3.2), which was subsequently orthorectified using the lidar dataset. The orthophoto consists of RGB channels and has a resolution of 0.25 m. Within the thesis the orthophoto is used as auxiliary and control dataset.

4 Methods

This chapter describes the applied methods for the extraction of features from the available DEM of the Monte Rosa east face. In the first section the preparation and visualisation of certain datasets of the Monte Rosa east face is delineated. The description of the methods is divided in two parts: section 4.2 details how *a priori* specified methods were applied to find out which features could be extracted (bottom-up approach; Figure 4.1). In section 4.3 those methodologies are described that were found to be convenient to extract the *a priori* specified features (top-down approach).

4.1 Preparation and visualisation of datasets

4.1.1 Preparation

Digital elevation model

In order to determine the influence of scale, grid resolutions of 1, 2, 5, 10, and 25 m of the available DEM were used in all analyses. The 1 m grid was generated from the lidar point cloud using an interpolation algorithm implemented in SCOP++ and made available for this study; the remaining grids were interpolated by the author using Natural Neighbour interpolation in ArcView®(ESRI, 2006).

Snow/ice and rock from orthophoto

As a reference basis, the snow and ice cover was manually digitized from the available orthophoto. The result is a vector layer that contains the two classes snow/ice and rock. The smallest polygon covers an area of about 300 m^2, smaller objects than this were not delineated. Hence, the created dataset does not exactly conform to the snow and ice cover represented in the orthophoto.

Section	4.2.1	4.2.3	4.2.2	4.3.1	4.3.2	4.3.2	4.3.3	
Features	-[a]	-	Snow/ice[b]		Steep fronts	Crevasses	Planes	
	↑	↑	↑	↓	↓	↓	↓	↓
Methods	Wood	Intensity	Roughness[b]		Edge detection[c]	Edge detection[c]	Wood	Brewer
Approach	**Bottom-up**			**Top-down**				

Fig. 4.1: Bottom-up approach leads from specified methods to features, and top-down approach from specified features to methods. [a]Since not the six morphometric features were the target features, no feature is mentioned. [b]Snow/ice and terrain roughness are part of both approaches. [c]Also includes spatial operations with the snow and ice cover.

4.1.2 Visualisation

For the visualisation of the results (chapter 5), ArcScene, part of the 3D Analyst extension of ArcView, was used. The raster datasets were draped over the elevation grid of corresponding resolution and were mostly illuminated with 315 degrees azimuth and 30 degrees altitude in order to facilitate recognising spatial context. A particular advantage of 3D towards 2D visualisation is, that regions with high slope are represented more naturally and accessible for the human eye. For flatter areas 2D is sufficient in most cases. A disadvantage of 3D is, however, that it is in general not possible to declare a correct measure and point of compass.

4.2 Specific methods to extract features (bottom-up)

Three approaches were chosen to be evaluated for their suitability for feature extraction from a steep alpine rock face: (1) the six morphometric classes by Wood (1996), (2) application of terrain roughness, and (3) of reflectance intensity.

4.2.1 The six morphometric classes by Wood (1996)

Fundamentals

Wood (1996) proposed a classification scheme that divides a DEM into six morphometric classes (or features): ridge, plane, channel, pit, peak, and pass (Figure 4.2). These can be derived through combinations of the second derivatives (Table 4.1, Wood, 1996), which are

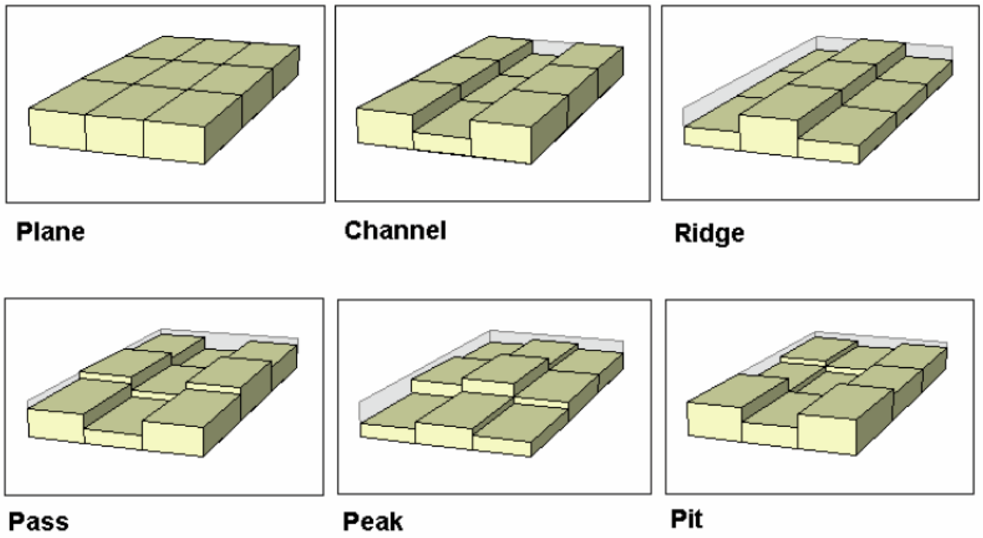

Fig. 4.2: Definition of the morphometric classes by means of a 3x3 focal window. From Wood (1996).

calculated as follows: a focal window is passed over the DEM, and the relationship between a central cell and its neighbours is examined using quadratic approximation (Evans, 1979; Wood, 1996). Whilst classification at a fixed window size is usual practice in geomorphometry, Wood (1996) proposed multi-scale classification using a range of window sizes to fully characterise a terrain surface. The multi-scale approach was later extended into fuzzy multi-scale classification based on the range of crisp classifications at different window sizes (Fisher et al., 2004).

Wood implemented his methods in LandSerf (Wood, 2007), a freely available GIS (Geographical Information System) for the visualisation and analysis of surfaces. According to the above stated explanations, three different approaches can be chosen for feature extraction (see Table 4.2 for an overview):

1. Single-scale feature extraction: the features are extracted using a specific window size, minimum 3x3.

2. Multi-scale feature extraction: the features are extracted using a range of window sizes. For instance, if window size 7x7 is chosen, analysis using window sizes 3x3, 5x5, and 7x7 is performed.

3. Fuzzy feature classification: based on multi-scale approach, the fuzzy membership of each of the six member classes is calculated, represented by values from 0 (not a

Feature name	Derivative expression	Description
Peak	$\frac{\delta^2 z}{\delta x^2} > 0, \frac{\delta^2 z}{\delta y^2} > 0$	Point that lies on a local convexity in all directions (all neighbours lower).
Ridge	$\frac{\delta^2 z}{\delta x^2} > 0, \frac{\delta^2 z}{\delta y^2} = 0$	Point that lies on a local convexity that is orthogonal to a line with no convexity/concavity.
Pass	$\frac{\delta^2 z}{\delta x^2} > 0, \frac{\delta^2 z}{\delta y^2} < 0$	Point that lies on a local convexity that is orthogonal to a local concavity.
Plane	$\frac{\delta^2 z}{\delta x^2} = 0, \frac{\delta^2 z}{\delta y^2} = 0$	Points that do not lie on any surface concavity or convexity.
Channel	$\frac{\delta^2 z}{\delta x^2} < 0, \frac{\delta^2 z}{\delta y^2} = 0$	Point that lies in a local concavity that is orthogonal to a line with no concavity/convexity.
Pit	$\frac{\delta^2 z}{\delta x^2} < 0, \frac{\delta^2 z}{\delta y^2} < 0$	Point that lies in a local concavity in all directions (all neighbours higher).

Table 4.1: Morphometric features described by partial second order derivatives. From Wood (1996).

member of a specific class) to 1 (full member).

If the rules in Table 4.1 were strictly applied, the resulting surface would consist almost entirely of channels and ridges, because (1) DEMs rarely hold truly planar objects with zero curvature and (2) true peaks, passes, and pits usually do not have an overall slope (Wood, 1996). Hence a curvature tolerance and a slope tolerance can be specified in LandSerf.

Application to the available DEM

Wood's classification method was applied to the DEM of the Monte Rosa east face in order to test the general suitability of this method for steep glaciated alpine rock faces. The method may turn out to be suitable for the extraction of specific relevant features.

The many combinations that result from (i) various grid resolutions of the input DEM, (ii) the three methods of feature extraction (Table 4.2), (iii) the arbitrary choices of the window size, and (iv) the choice of curvature tolerance and slope tolerance, lead to a very large number of analysis possibilities. In order to limit these to a reasonable amount, the following basic conditions were chosen:

- As in the other approaches within this work, the DEM was analysed with the grid resolutions 1, 2, 5, 10, and 25 m.

	Method	Description	Output	Window size	LandSerf menu navigation
1	Feature extraction	Extraction of the 6 features at a specific scale (neighbourhood window)	Grid classified into the 6 morphometric classes at a specific scale	≥ 3	Analyse > Surface parameter > Feature extraction
2	Multi-scale feature extraction	Extraction of the 6 features considering multiple scales (range of neighbourhood windows)	(a) Grid showing mode of multi-scale feature classifications (b) Grid showing scaled entropy of multi-scale feature classifications	> 3	Analyse > Multi-scale parameter > Feature extraction
3	Fuzzy feature classification	Calculation of fuzzy membership (range of neighbourhood windows)	6 grids showing membership of the 6 features	> 3	Analyse > Fuzzy feature classification

Table 4.2: Three methods available in LandSerf to extract the six morphometric features ridge, plane, channel, pit, peak, and pass.

- Since curvature tolerance and slope tolerance exert a dominating influence on the type of the features that are extracted, different settings were applied (with the 5 m resolution grid): curvature tolerance: 0.1 (default) and 0.5; slope tolerance: 1 ° (default) and 40 °.

The multi-scale feature extraction and fuzzy feature (multi-scale) classification (methods 2 and 3 in Table 4.2) were omitted because the influence of scale is already rudimentarily covered by the different resolutions of the input DEMs.

4.2.2 Application of terrain roughness

The application of terrain roughness presents another bottom-up approach, with which possible relevant features may be extracted.

Fundamentals

Terrain roughness is a complex statistical land-surface parameter, and there is no clear agreement on how to measure roughness (see sec. 2.2.2). Here the method Vector Ruggedness[1] Measure (VRM; Sappington et al., 2007) was used because it is more independent of slope than other approaches. It measures roughness by quantifying the dispersion of vectors or variation in slope and aspect across a neighbourhood window (Fig. 4.3). The procedure of VRM is described in Sappington et al. (2007). Unit vectors normal to each grid cell are decomposed into their x, y, and z components using the slope and aspect of the cell. Then the resultant vector over a cubic neighbourhood (e.g. 3x3x3) is calculated centred on each cell, using a moving analysis window. The vector magnitude is divided by the number of

[1] Ruggedness is sometimes used as synonym for roughness.

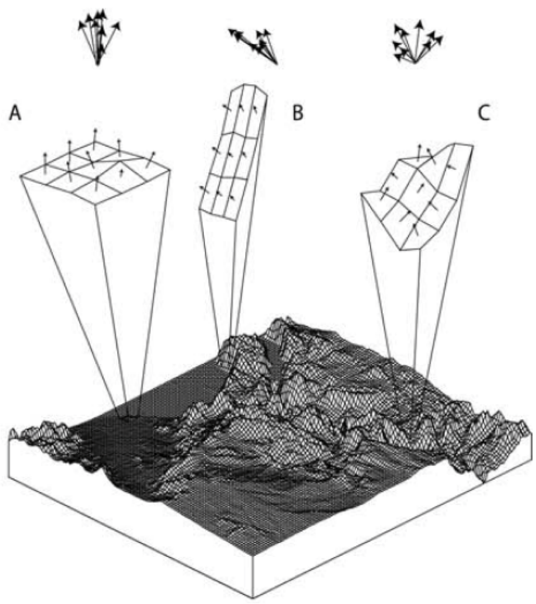

Fig. 4.3: Illustration of Vector Ruggedness Measure (VRM). In flat (A) and steep areas (B), both smooth, the VRM values are low; in rough areas (C) values are high. Sketch from Sappington et al. (2007).

cells in the neighbourhood to obtain the magnitude of the resultant vector in standardized form, which is a measure of the roughness of the land surface for the selected scale (window size) (Sappington et al., 2007; Hobson, 1972). This magnitude is subtracted from 1, leading to a dimensionless number that ranges from 0 (flat) to 1 (most rough). A script for the calculation of VRM in ArcView is freely available for download (Sappington, 2008).

Correlation of roughness and slope

Depending on the calculation method, roughness can strongly correlate with slope (e.g. standard deviation; Olaya, 2008). Therefore, Sappington et al. (2007) compared the dependence of VRM and two other roughness calculation methods and correlated the results with slope. They found that VRM shows the least correlation with slope. Furthermore, they demonstrated that the correlation is dependent on the characteristics of the area: the calculated Spearman rank correlation coefficients — measuring the relationship between two variables — yielded 0.31, 0.42, and 0.71 for three different mountain ranges.

The Monte Rosa east face differs from the above named three areas in the sense that it is not a mountain range but a rock face; it is not known if VRM is decoupled from slope also in this landscape type. Hence the Spearman rank correlation coefficient of VRM and slope was evaluated before further analysis with terrain roughness. This was done in *R* (R Development Core Team, 2008), a language and environment for statistical computing and graphics.

Application to the available DEM

The roughness of the available DEM was calculated using the VRM method with multiple grid resolutions (1, 2, 5, 10, and 25 m) and for the 1 m grid resolution additionally with multiple window sizes (3x3, 11x11, and 25x25).

4.2.3 Application of reflectance intensity

The reflectance intensity of the lidar data was visualised in order to decide if it can be used for feature extraction from a steep alpine rock face. For the visualisation of the intensity values a list of the (non-gridded) lidar point cloud with the attributes x,y,I (I = intensity) was prepared, which was then interpolated with Natural Neighbour interpolation in ArcView to a 1 m grid representing the intensity values.

As described in section 5.1.3 the reflectance intensity of the on hand lidar data is not adequate for feature extraction, hence no further analysis was performed.

4.3 Extraction of specific features (top-down)

It was attempted to extract four specific feature types — snow/ice, steep fronts, crevasses, and geological/geomorphological planes — from the available DEM, using approaches that are described in the following.

4.3.1 Snow and ice cover

The goal was to extract snow/ice solely from a DEM, without using auxiliary datasets such as an orthophoto.

Identifying different surface coverages

Only considering the terrain surface, the obvious difference between snow/ice and rock is the roughness of the surface: snow and ice are usually smoother than rock. Hence the statistical land-surface parameter terrain roughness was chosen for the differentiation of snow/ice and rock into two classes. For the calculation the method Vertical Ruggedness Measure (VRM) was applied (see sec. 4.2.2 for a detailed description of VRM).

	Predicted (terrain roughness)	
Actual (orthophoto)	Rock	Snow/ice
Rock	a	b
Snow/ice	c	d

Table 4.3: Confusion matrix with the two classes snow/ice and rock. *Predicted* complies with the values from terrain roughness calculations, *actual* with those from the orthophoto. For an explanation of the matrix entries see text.

Three combinations of grid resolution and window size (1 m resolution with 3x3 and 25x25 window sizes, and 5 m resolution with 3x3 window size) were used for the calculation of roughness, which resulted in three different grids, each representing roughness values between 0 and 1.

Quantify and optimise result with a confusion matrix

In order to determine which threshold value best divides the roughness grids into the classes "not rough" (or rather "snow/ice") and "rough" (or rather "rock"), the roughness grids were compared with the manually generated snow/ice and rock classes from the orthophoto using a confusion matrix (Kohavi and Provost, 1998). A confusion matrix is a means of evaluating classifiers, with the classifier being terrain roughness in this case. The entries in the confusion matrix have the following meaning in the context of this study (Table 4.3):

- a is the number of *correct* predictions that a grid cell is *rock*
- b is the number of *incorrect* predictions that a grid cell is *snow/ice*
- c is the number of *incorrect* of predictions that a grid cell is *rock*
- d is the number of *correct* predictions that a grid cell is *snow/ice*.

The accuracy (AC) of the classification — the proportion of the total number of predictions that were correct — can be calculated using the following formula (Kohavi and Provost, 1998):

$$AC = \frac{a+d}{a+b+c+d} \tag{4.1}$$

However, if the number of negative cases is greater than the number of positive cases, AC loses its validity (Kubat et al., 1998).

The following steps were conducted in order calculate the accuracy of the classificator terrain roughness for the three above named roughness grids representing multiple scales:

1. *Choose a roughness threshold:* this threshold determines, how high a cell value has to be in order to count as rock.

2. *Obtain the actual snow/ice and rock values from orthophoto:* The manually created polygon vector layer comprising the two classes "snow/ice" and "rock" was converted to two grids (1 and 5 m resolution) with the cell values of snow/ice being 0 and rock being 1. This step had only to be done once.

3. *Obtain the values a, b, c, and d of the confusion matrix:* Since both the predicted (roughness) and the actual snow/ice and rock classes (from orthophoto) were available as grids in the meantime, the values a, b, c, and d could be assessed and stored in a new raster dataset through map algebra. The quantity of a, b, c, and d cells was determined using raster statistics.

4. *Obtain accuracy:* with the now available quantity of values a, b, c, and d, the accuracy of the classification into snow/ice and rock predicted by terrain roughness was calculated according to equation 4.1.

This procedure was conducted at different roughness thresholds (see Table 5.2) and at three different scales (three roughness grids), in order to obtain the maximum accuracy and the most adequate scale.

Analysing "rough" edges

The visualisation of the above calculated snow/ice cover reveals, that not only rough surface but also coarse-scaled edges such as ridges and channels were identified as rough, including those made of snow/ice (see sec. 5.2.1). While rough rock edges can be tolerated (since rock is rough anyway), snow/ice edges should not be identified as rough. Therefore, it was attempted in the following step, to isolate the snow/ice edges from the rock edges.

It was assumed that the influence of scale on rock edges is different from that on snow/ice edges, which would imply that it is possible to filter out snow/ice edges. In order to test this hypothesis, the following procedure was applied:

1. VRM of the 1 m DEM with window sizes 3x3, 5x5, 11x11, and 25x25 was calculated[2], resulting in four grids expressing the roughness at each scale.

2. A roughness threshold value of 0.01 was chosen as being appropriate, with the cell values above this value counting as rough.

[2]Window sizes were chosen analogue to the grid resolutions 1, 2, 5, 10, and 25 m, whereas 1 and 2 m are not valid window sizes and are therefore not considered, and 11 instead of 10 m was chosen because window sizes must be odd numbers.

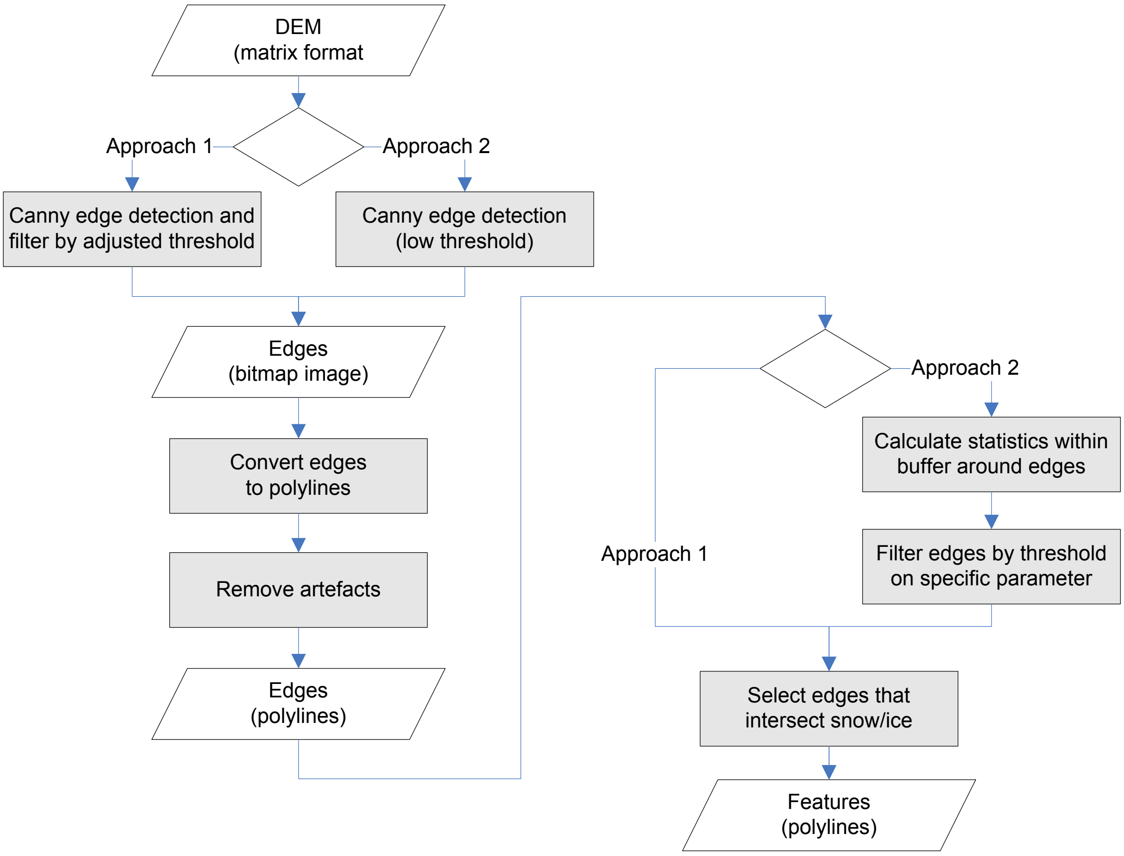

Fig. 4.4: Flow diagram representing the applied procedure for the extraction of steep fronts and crevasses. Two different approaches were evaluated.

3. A Python script conducting geoprocessing and raster calculation in ArcView was written that takes these four roughness grids of different scales and the above defined roughness threshold as input and generates one new raster grid that shows the roughness of the DEM over a range of scales.

The cell values of that grid were coded as binary numbers where the last digit indicates if the DEM is rough (0 or 1) at the smallest window size (here 3x3), the second last digit indicates if the second smallest window size is rough (here 5x5), and so on. For instance, a cell value of “1100” indicates that the DEM is only rough at the two greater window sizes (11x11 and 25x25) according to the above specified threshold value.

4.3.2 Steep fronts and crevasses

For the extraction of steep fronts and crevasses a similar procedure was applied, which is illustrated in Figure 4.4.

Identifying linear features

Both steep fronts and crevasses are characterised by variations or discontinuities in elevation. The most basic method to recognise variation of elevation is by calculating the focal slope angle per pixel and to apply a threshold value to distinguish pixels with high from those with low slope. Issues of this method are that — in general — one does not obtain discrete objects, but single pixels reflecting data noise or aggregated pixels forming areas that sometimes contain holes or are not connected where it would be obvious.

In order to obtain discrete, connected, linear objects, edge detection methods have been considered. Originally, edge detection is a terminology from image processing and has been used to detect local discontinuities of image intensity (Pitas, 1993). Assigned to DEMs, local discontinuities of elevation — thus slopes — are detected. Well-known edge detection operators are Sobel and Prewitt. Both these operators define an edge as a vector, with the edge direction being perpendicular to the up-slope direction (Mason et al., 2006). Using these operators indeed leads to discrete edges, which, however, are very short and often not linked where it would be obvious. In order to solve this problem Canny (1986) developed the Canny operator, which uses hysteresis thresholding, a simple yet effective way to link edge segments (Mason et al., 2006). Due to the advantages in contrast to the other operators, the Canny operator was chosen here for the extraction of edges.

Canny edge detector

For a better insight into the functionality of the Canny operator, a short summary is given in the following. For a more detailed description see Canny (1986).

1. *Suppress noise:* a Gaussian convolution mask[3] is applied to reduce noise and detail (Gaussian blur filter).

2. *Detect edges:* edges are detected using the Sobel operator, which calculates the absolute gradient (i.e. the difference between two neighbouring pixels) to locate discontinuities. It uses a pair of 3x3 convolution masks, one estimating the gradient in x direction and one in y direction (see equations 4.2 and 4.3, resp.; A = focal DEM matrix; S_x, S_y = Sobel operator matrix in x and y direction; G_x, G_y = gradients in x and y direction). The magnitude of the gradient is the sum of the x and y gradient

[3] A convolution mask is a one- or two-dimensional matrix whose values represent weights. The matrix values are multiplied by the pixel values and added together. The result is stored at the centre of the matrix. The mask is moved pixel by pixel and the operation is repeated until the image is completely processed.

(G in equation 4.4). If the gradient is greater than a user-defined threshold the pixel counts as an edge.

3. *Classify edge directions:* the detected edges are classified into the 0, 45, 90, or 135 ° direction. For instance, any edge falling into the range 22.5 to 67.5 ° is set to 45 °.

4. *Thin out edges:* non-maximum suppression is applied, which eliminates possible wide ridges, leading to single response to edges.

5. *Obtain connected edges:* hysteresis is used as a means of eliminating streaking. Streaking is the breaking up of an edge when signal response is fluctuating just under and above a threshold, potentially resulting in a dashed line. In order to avoid streaking, hysteresis uses two thresholds, a higher (T1) and a lower one (T2). Any pixel that is above T1 is presumed to be an edge pixel. Any pixels that are connected to edge pixels and that have a greater value than T2 are also selected as edge pixels. Figuratively speaking, an edge starts if the value is greater than T1 and ends as soon as the value is lower than T2.

$$G_x = S_x * A = \begin{bmatrix} 1 & 0 & -1 \\ 2 & 0 & -2 \\ 1 & 0 & -1 \end{bmatrix} * A \tag{4.2}$$

$$G_y = S_y * A = \begin{bmatrix} 1 & 2 & 1 \\ 0 & 0 & 0 \\ -1 & -2 & -1 \end{bmatrix} * A \tag{4.3}$$

$$G = \sqrt{{G_x}^2 + {G_y}^2} \tag{4.4}$$

Application to the available DEM

The procedure for the extraction of steep fronts from the DEM is illustrated in Figure 4.4. For the extraction of steep fronts, the DEM was analysed with 1–25 m cell sizes; due to the small dimension of crevasses, their extraction was investigated with the 1 m DEM only. Canny edge detection was carried out using the *edge* function of the Image Processing Toolbox in MATLAB®(The MathWorks, 2007). For this purpose, the DEM had to be converted into matrix format.

Two different approaches were used that differ in edge filtering (Fig. 4.4):

- *Approach 1 — filtering by edge detection:* Canny edge detection was applied with the gradient threshold T1 being adjusted in order that only edges representing four sample steep fronts (1, 6, 7, and 8 in Fig. 3.3) or eight sample crevasses (Fig. 5.12) were just being detected.

- *Approach 2 — filtering by zonal analysis:* Canny edge detection was used with a low threshold T1 of 0.0005 (steep fronts) or 0.0002 (crevasses). In order to filter out the minor elevation discontinuities and to attempt to keep only those polylines representing the desired features (steep fronts or crevasses), the following procedure was applied. Around each edge buffers were calculated. For the 1 m grid buffer sizes of 1, 2, 5, 10 and 25 m (steep fronts) or only 1 m (crevasses) were chosen. For the remaining grid resolutions (steep fronts only) a buffer size matching the cell size was used. Within the buffers, zonal statistics were calculated including range of elevation (DIFF), standard deviation of elevation (STD), mean slope angle (MEAN_SL), and maximum slope angle (MAX_SL), in an attempt to characterise, that is to say to extract steep fronts with at least one of those parameters.

In both approaches, the threshold values (of the gradient in approach 1 and of the parameters in approach 2) were chosen at which the sample features were just being selected and at which as few other features as possible for each feature type (steep front or crevasse) were being included. These values were considered the best to use for extracting the corresponding feature type.

In the following, some information about edge detection in MATLAB and about obtaining vector polyline features is given. The lower threshold T2 is determined by MATLAB as $0.4 * T1$. The size of the filter window is chosen automatically. As a result a bitmap image with the values 0 and 1 is generated where the value 1 represent the edges. The edges in the bitmap image were converted into vector polylines using ArcView. The obtained polylines did not only represent the favoured features (steep fronts or crevasses), but also edges of other elevation discontinuities and artefacts. Some of the latter could be removed manually, for instance the border of the DEM.

Within both approaches, and as a last step, the remaining edges were spatially filtered. Those edges intersecting the snow/ice polygons (see sec. 4.1.1) were designated as steep fronts; those being completely inside the snow/ice polygons were marked as crevasses.

As will be shown in chapter 5, the above procedure provided good results regarding steep fronts, but the results for crevasses were not as good.

4.3.3 Geological planes

For the extraction of geological/geomorphological planes from a DEM two different approaches were evaluated: (1) classification of slope and aspect by Brewer and Marlow (1993) and (2) extraction of the morphometric class plane by Wood (1996). The analyses of the DEM were performed with the grid resolutions 1, 2, 5, 10, and 25 m. The results were compared to three visually identified planes.

Identifying planes

(1) Classification of slope and aspect Brewer and Marlow (1993) developed a method for the colour representation of slope and aspect simultaneously. This method classifies a DEM into 25 colour classes based on combinations of slope and aspect.

The method was adapted for use in this work — as shown subsequently — and carried out in ArcView. The accomplished steps are shown in Figure 4.5. First, slope and aspect were calculated. Aspect was then divided into eight classes: N (337–22 °), NE (22–67 °), E (67–112 °), etc.; slope was divided into four classes, with the flattest eight aspect classes combined to one. Originally, the slope classes were configured for a maximum slope of 220 percent rise[4] (∼65.6 °); due to the very steep slopes of the Monte Rosa east face, the maximum slope was increased to 90 °, resulting in the four slope classes 0–22.5 °, 22.5–45 °, 45–67.5 °, 67.5–90 °.

The classified slope and aspect grids were summed, leading to a grid with values 19–48, where the first digit indicates the slope magnitude (with 1 being flat, 2 low, 3 medium, and 4 high), and the last digit indicates the aspect orientation (with 1 being north, 2 northeast, 3 east, etc.). As mentioned above, the flattest eight aspect classes (numbers less than 20) were combined to one class (19).

Originally, the method has some more steps relating to colour representation, which are not relevant in this context. However, RGB values for the classes are provided, which were borrowed for the visualisation.

(2) Extraction of Wood's morphometric class plane The classification method by Wood was considered as a possible solution for the extraction of geological/geomorphological planes, since it is able to identify planar features (for more details on Wood's method see sec. 4.2.1). Feature extraction with fixed 5x5 window size and curvature tolerance of 0.5

[4] Brewer and Marlow (1993) used percent rise for slope calculation.

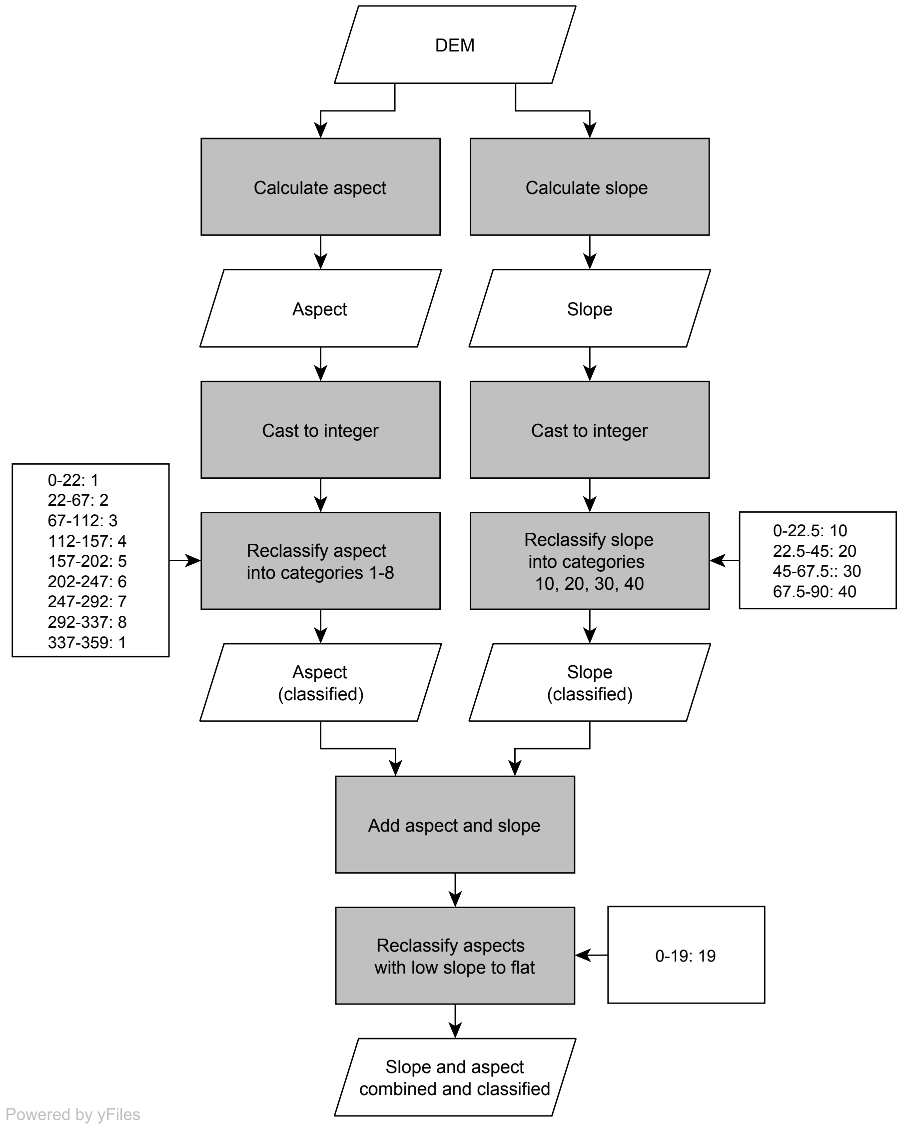

Fig. 4.5: Procedure for the classification of the DEM into 25 slope/aspect categories on the basis of Brewer and Marlow (1993).

was applied with the 10 m DEM. A grid with six different values was obtained, one of them representing the morphometric class *plane* (method 1 in Table 4.2).

5 Results

The results of feature extraction using different methods from the available DEM of the Monte Rosa east face are presented here. This chapter is similarly structured to the Methods chapter. The results are discussed in the next chapter.

5.1 Application of specified methods (bottom-up approach)

In this section the suitability of the previously specified methods for feature extraction from a DEM representing an alpine rock wall is examined and, if applicable, it is shown what kind of features can be identified.

5.1.1 The six morphometric classes by Wood (1996)

The results of the classification of the DEM into the six morphometric classes ridge, plane, channel, pit, peak, and pass with different grid resolutions are illustrated in Figure 5.1. Only the feature types ridge, channel, and plane were identified. The decrease of grid resolution from 1 to 25 m results in a gain of the ridge and channel fraction at the cost of planar cells (Table 5.1). At finer scales small features such as channels are recognised, though the identification of large structures such as mountain ridges does not work; features of this type can in contrast be seen at coarser scales. A comparison with the orthophoto shows that the snow and ice cover is highlighted by the planar class. Although the large ridges

Cell size [m]	Ridge [%]	Plane [%]	Channel [%]
1	32.7	33.6	33.7
2	37.9	22.1	40.0
5	39.5	17.6	43.0
10	40.1	14.7	45.2
25	41.1	10.5	48.4

Table 5.1: Proportions of the ridge, channel, and planar fractions. The remaining three classes hardly occur and are thus not included

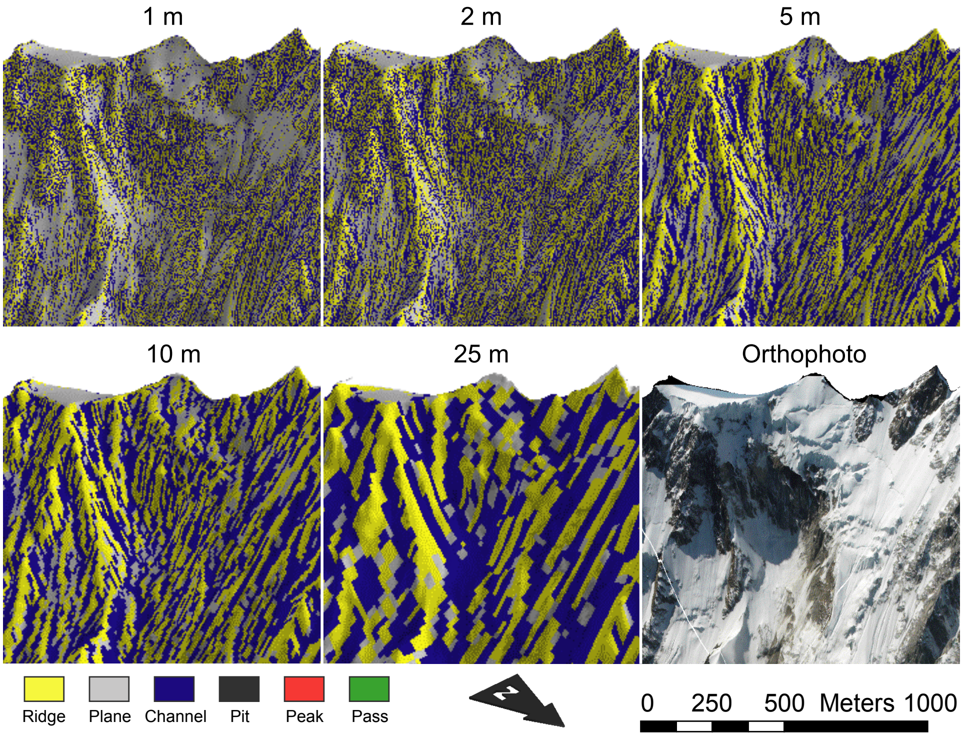

Fig. 5.1: Classification of the available DEM of different grid resolutions (1, 2, 5, 10, and 25 m) into the six morphometric classes by Wood (1996). Feature extraction settings: window size: 3x3; slope threshold: 1° (default); curvature 0.1 (default). Extent see quadrangle A in Figure 5.2.

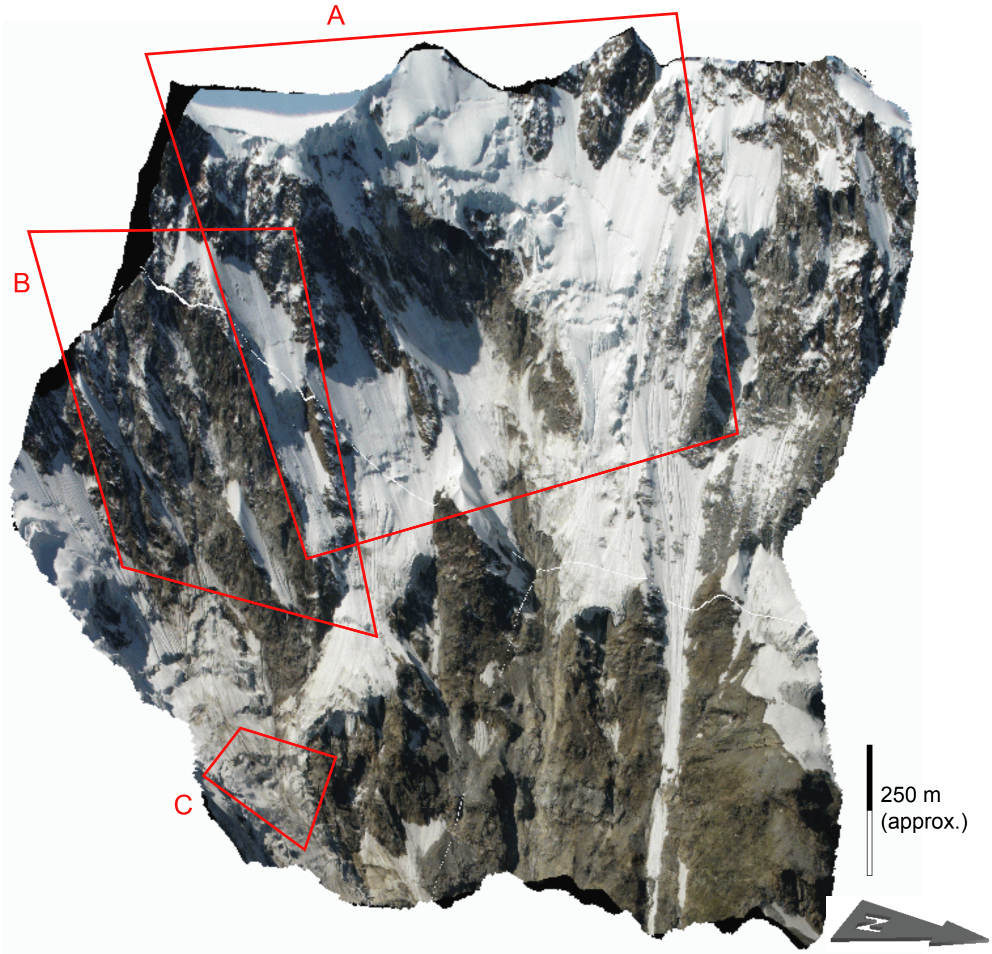

Fig. 5.2: Orthophoto draped over the 1 m DEM. The extent of Figures 5.1, 5.3, 5.5 is marked by quadrangle A, the one of Figure 5.15 by quadrangle B, and the one of Figure 5.12 by quadrangle C. The quadrangles are distorted due to different view perspectives.

and channels are accentuated at coarser scales (for instance the channel below the Parete Innominata, Fig. 3.2), many more areas are classified as channels and ridges, although they would not be seen as such using "common sense".

Adjustment of the default slope and curvature tolerance values lead to notable differences in the results (Fig. 5.3). The increase of curvature tolerance resulted in more planar cells and less ridge and channel cells. In this way, rather smooth surfaces such as snow and ice cover tended to be identified as planar.

The increase of the slope tolerance showed a different effect and resulted in more cells being identified as peak, pit, or pass (Fig. 5.3). This effect is more striking at a lower curvature tolerance. Naturally, a very high slope tolerance, as chosen in Figure 5.3, leads to cells being classified as peak, pit, or pass, which are not necessarily any of these.

5.1.2 Application of terrain roughness

Terrain roughness was considered as a possible means of extracting features (e.g. different surface covers) from the available DEM. In a first step, the results of the suitability of the used roughness calculation method for steep walls are presented, whilst in a second step the suitability of roughness itself for feature extraction is evaluated.

Correlation of roughness and slope

The Vector Ruggedness Measure (VRM) is claimed to be independent of slope in mountain ranges (Sappington et al., 2007). In order to test if this characteristic is also true for alpine steep flanks, the correlation of VRM and slope was tested for the available DEM. A Spearman's rank correlation coefficient of 0.38 was calculated, which lies within the findings of Sappington et al. (2007) and indicates that those two variables are relatively independent (Fig. 5.4). Therefore, VRM was confirmed as being independent of slope.

Roughness of the available DEM

Terrain roughness was calculated with different window sizes and grid resolutions, the results of which are illustrated in Figure 5.5. Bedrock areas are measured as rough, which is particularly true for finer scales. As scale becomes coarser, edges (particularly ridges) obtain high roughness values at the cost of rocky areas in general. In fact, VRM seems to predominantly recognise edges as rough. At finer scales (high resolution and small window size) edges of the whole range of scales are identified, such as fine-scale irregularities, particularly existing in rocky areas, as well as coarse-scaled ridges, channels and steep fronts.

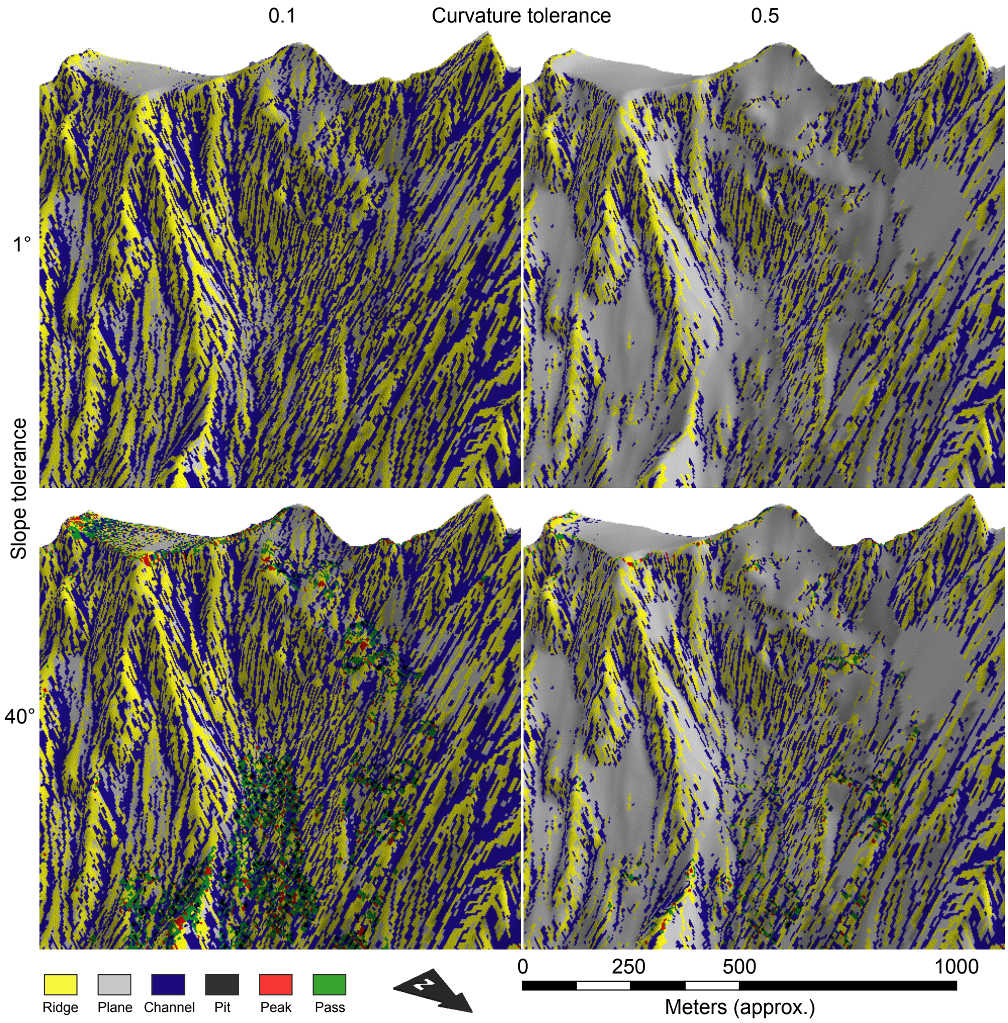

Fig. 5.3: Classification of the available DEM into the six morphometric classes by Wood (1996) using different slope and curvature tolerances. Grid resolution: 5 m. Extent see quadrangle A in Figure 5.2.

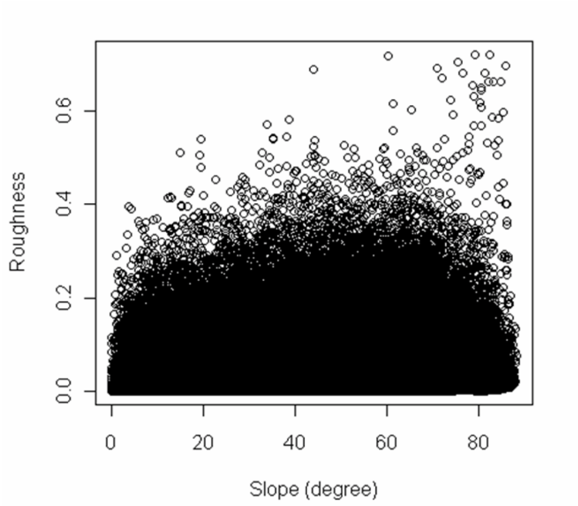

Fig. 5.4: Scatter plot of roughness (VRM) and slope, which does not indicate a significant relationship between the two variables.

At coarser scales, only coarse-scaled features are identified, highlighted by broad bands of high roughness. In general, terrain roughness decreases as scale becomes coarser. Thus, the maximum roughness of the 1 m DEM amounts to 0.74 and of the 25 m DEM to 0.24, whereas from the 1 m to the 2 m DEM (both calculated with a 3x3 analysis window) the maximum roughness increases (from 0.74 to 0.78).

The above mentioned coherence between rock and roughness was applied in the attempted differentiation of rock and snow/ice within this work (see sec. 5.2.1).

5.1.3 Application of reflectance intensity

In the reflectance intensity grid the flight stripes of the laser scanning procedure are clearly visible (Fig. 5.6). It is noticeable that the snow/ice cover shows locally higher values than rock (e.g. in the area of Dufourspitze). However, in order to use intensity globally for feature extraction, the data would have to be corrected (e.g. Höfle and Pfeifer, 2007).

5.2 Extraction of specific features (top-down)

In this section the results of the extraction of the previously specified features snow/ice, steep fronts, crevasses, and geological/geomorphological planes are presented.

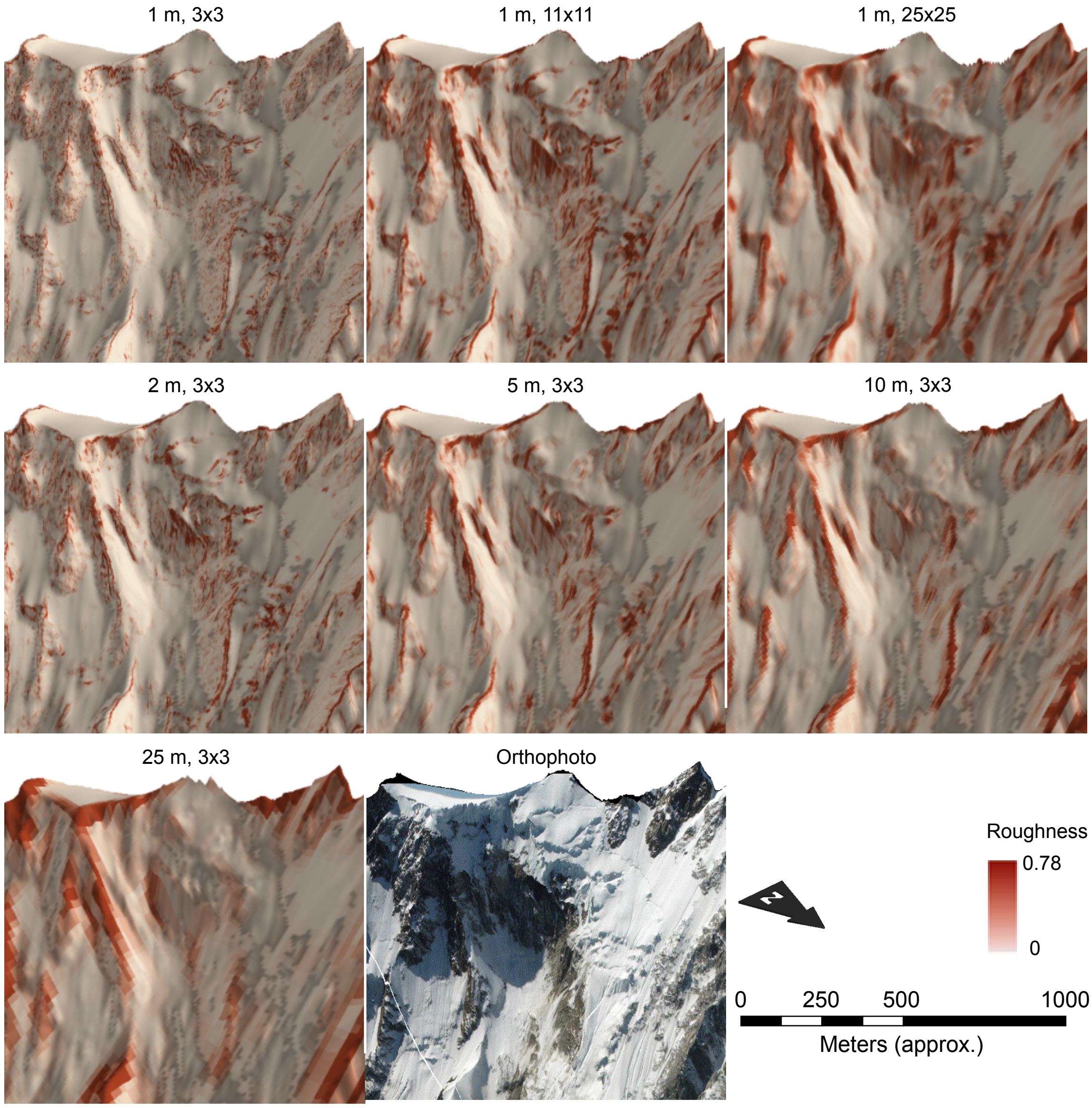

Fig. 5.5: Terrain roughness (VRM) of the available DEM with different window sizes (1. row) and different grid resolutions (2. and 3. row). Maximum roughness (top left to bottom right): 0.74, 0.54, 0.45, 0.78, 0.52, 0.41, 0.24. The roughness legend is relative and adapted at each sample. Scale applies approximately for bottom of figure.

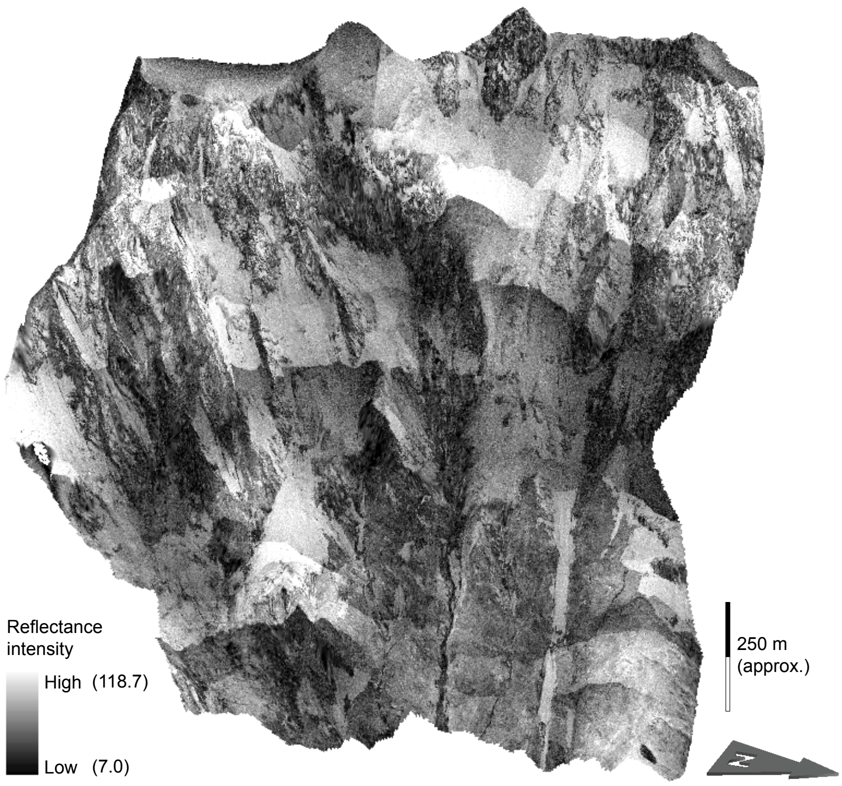

Fig. 5.6: Reflectance intensity of the available lidar data. Interpolated to a 1 m raster grid and draped over the DEM. Horizontal stripes relate to the flight lines. Here, the DEM is not shaded.

No.	Grid res.	Window size	Roughness threshold	*a* (pos. as rock)	*b* (neg. as rock)	*c* (neg. as snow/ice)	*d* (pos. as snow/ice)	$a+d-b+c$ (pos.-neg.)	Accuracy
1	1 m	3x3	0.01	282’570	168’284	1’272’677	1’539’828	381’437	0.56
2	1 m	3x3	0.1	4’454	5’293	1’550’793	1’702’819	151’187	0.52
3	1 m	3x3	0.05	20’400	20’874	1’534’847	1’687’238	151’917	0.52
4	1 m	3x3	0.005	568’343	296’753	986’904	1’411’359	696’045	0.61
5	**1 m**	**3x3**	**0.001**	**1’240’944**	**709’599**	**314’303**	**998’513**	**1’215’555**	**0.69**
6	1 m	3x3	0.0002	1’503’762	1’176’675	51’485	531’437	1’128’997	0.62
7	1 m	3x3	0.0005	1’399’198	911’132	156’049	796’980	499’295	0.67
8	1 m	3x3	0.0001	1’535’974	1’362’759	19’273	345’353	807’039	0.57
9	1 m	3x3	0.002	993’366	517’363	561’881	1190’749	807’039	0.67
10	1 m	25x25	0.001	1’526’519	1’520’098	12	137’591	144’000	0.52
11	1 m	25x25	0.01	1’439’710	966’667	86’821	691’022	1’077’244	0.67
12	**1 m**	**25x25**	**0.02**	**1’246’744**	**683’419**	**279’787**	**974’270**	**1’257’808**	**0.70**
13	1 m	25x25	0.03	1’014’100	506’641	512’431	1151’048	1’146’076	0.68
14	1 m	25x25	0.05	623’401	302’941	903’130	1’354’748	772’078	0.62
15	1 m	25x25	0.1	185’330	103’801	1341’201	1’553’888	294’216	0.55
16	5 m	3x3	0.02	15’912	9’264	48’811	64’836	22’673	0.58
17	5 m	3x3	0.001	61’118	48’776	3’605	25’324	34’061	0.62
18	5 m	3x3	0.0001	64’095	68’805	628	5’295	-49	0.50
19	5 m	3x3	0.005	44’696	25’564	20’027	48’536	47’641	0.67
20	5 m	3x3	0.007	37’923	20’912	26’800	53’188	43’399	0.66
21	5 m	3x3	0.006	41’059	22’982	23’664	51’118	45’531	0.66
22	5 m	3x3	0.003	52’629	33’057	12’094	41’043	48’521	0.67
23	**5 m**	**3x3**	**0.004**	**48’443**	**28’768**	**16’280**	**45’332**	**48’727**	**0.68**

Table 5.2: Accuracy of terrain roughness (VRM) for the extraction of snow/ice. Three different basic conditions (combinations of grid resolution and window size for roughness calculation) were applied. The roughness threshold was iteratively adjusted to find the maximum accuracy for each basic condition (best result of each basic condition is highlighted in table). Columns *a*, *b*, *c*, and *d* represent the fields in the confusion matrix and contain the number of cells: *a* = cells that are positively predicted as rock; *b* = negatively predicted as rock; *c* = negatively predicted as snow/ice; *d* = positively predicted as snow/ice. Positively predicted cells have to outnumber negative ones in order to assure meaningful accuracy values, that is to say the entry in column $a+d-b+c$ has to be positive.

5.2.1 Snow and ice cover

In section 5.1.2, terrain roughness (VRM) was indicated as a possible means of differentiating between snow/ice cover and rock. Accordingly, terrain roughness was considered as a possible method to distinguish snow/ice and bedrock. In this section, the results of this evaluation are presented.

Quantifying the result

The evaluation of terrain roughness as a means of differentiating snow/ice and rock using the orthophoto for comparison showed at best an accuracy of 68–70 % with the three applied basic conditions (combinations of grid resolution and analysis window size; Tab. 5.2). Based on the fact that the maximum accuracy is similar in all three basic conditions, the accuracy does not seem to be strongly dependent on scale. However, the roughness thresh-

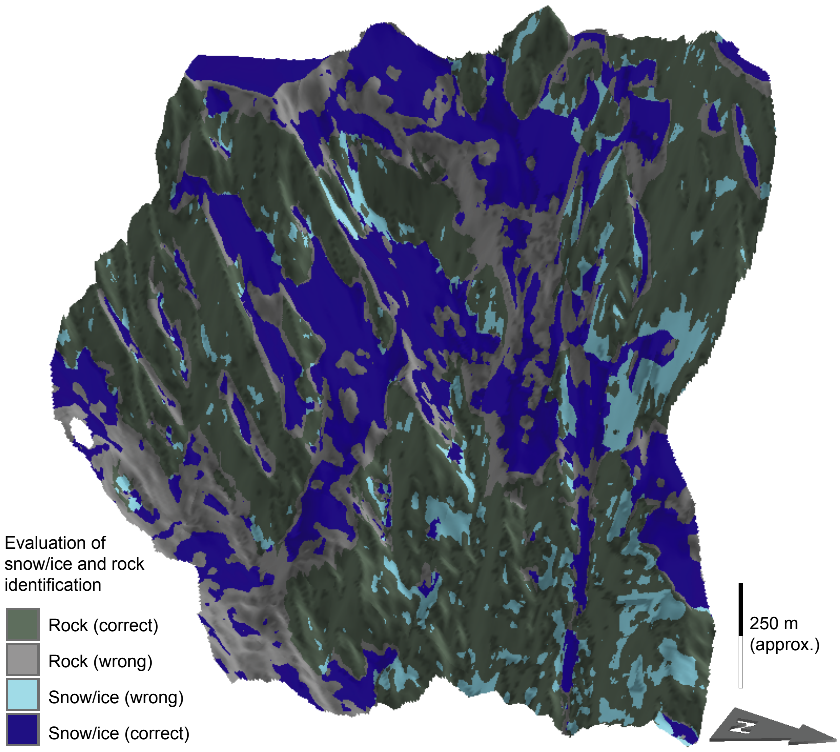

Fig. 5.7: Visual evaluation of the identification of snow/ice and rock with terrain roughness, based on the results of a confusion matrix. Framework conditions: 1 m DEM, 25x25 window size, and roughness threshold of 0.02 (no. 12 in Table 5.2). The terms "correct" and "wrong" relate to the cells that are correctly or wrongly predicted as rock or snow/ice by terrain roughness. Accordingly, snow/ice in the orthophoto complies with "Snow/ice (correct)" and "Rock (wrong)", and rock in the orthophoto complies with "Rock (correct)" and "Snow/ice (wrong)".

old, which indicates how high the value of a cell has to be in order to count as rough, varies with changing grid resolution and window size; the roughness threshold that leads to the best accuracy, was found on iterative approach.

The entries of the confusion matrix of the best accuracy (no. 12 in Tab. 5.2) are visualised in Figure 5.7. It becomes clear that the main reason for the relatively low accuracy of 70 % is the fact that snow/ice is often wrongly identified as rock, when steep fronts or irregularities in the snow/ice cover occur. In order to evaluate whether these rough snow/ice areas can be identified and hence marked as "not rough", the scale-dependence of roughness of snow/ice was analysed more precisely, in an attempt to improve the method through a multi-scale approach.

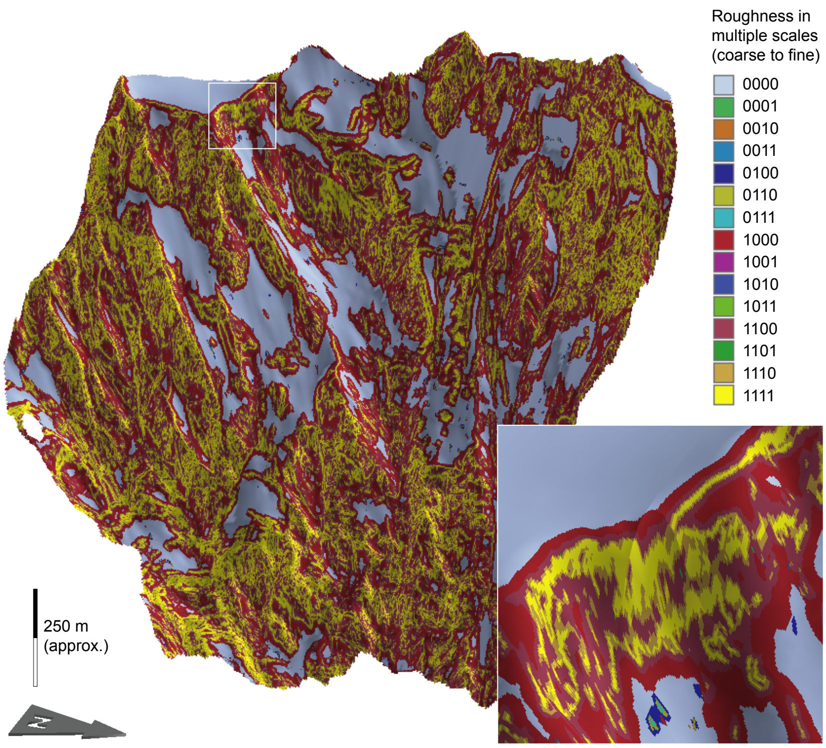

Fig. 5.8: Simultaneous visualisation of terrain roughness at four scales (window sizes), measured at the 1 m DEM. Legend: digits represent roughness calculated with the window sizes 3x3, 5x5, 11x11, and 25x25 (from right to left); 1 = rough, 0 = not rough in the according scale. Roughness threshold = 0.01. Detail: edge, here steep front, is seen as rough in all scales (1111).

Scale-dependence of terrain roughness

The result of the scale-dependence of roughness is illustrated in Figure 5.8. The sixteen classes represent all possible variations of roughness at four different analysis window sizes. The name of each class indicates with the binary values "1" (true or rough) and "0" (false or not rough) at which analysis window size a cell is measured as rough. For instance, the cells of the class "0000" are not seen as rough in any of the four window sizes, whereas "1100" comprises all cells that are measured as rough using the two larger analysis windows.

With the used window sizes, no general difference can be seen between the roughness of the irregularities within rock or of those within snow/ice: according to this, snow/ice edges such as steep fronts (see detail in Fig. 5.8) are seen as rough at all scales, like rock edges, and can therefore not be differentiated from these.

5.2.2 Steep fronts

The four *a priori* visually observed steep fronts (1, 6, 7, and 8 in Fig. 3.3) acted as a benchmark for finding a method for the extraction of steep fronts. Two different approaches were evaluated: (1) use of Canny edge detection only, and (2) use of Canny edge detection and zonal analysis.

Approach 1: filtering by edge detection

This led to 18–47 found edges (artefacts excluded), depending on the resolution (see column "Edges (thresh)" of no. 33–37 in Tab. 5.3). The further procedure, which includes intersection with snow/ice, is outlined below.

Approach 2: filtering by zonal analysis

With the Canny operator using a threshold of 0.0005 75–5026 edges were detected (artefacts excluded), depending on the resolution of the DEM (column "Total edges" in Tab. 5.3).

The number of the edges that were obtained through the filtering of the determined parameter thresholds varies from 19 (column "Edges (thresh)" of no. 24 and 32 in Tab. 5.3) up to several hundred, depending on the combination of grid resolution, buffer size, and the parameter.

Intersecting with snow/ice

Both above described approaches provided edges, which still did not represent uniquely steep fronts. Some edges lie within rocky areas, which does not usually apply for steep fronts (e.g. see "Edges that match threshold" in Fig. 5.11). Hence, the edges were filtered and reduced in a further step by spatial intersection of the edges and the snow/ice cover (column "Edges (snow/ice)" in Tab. 5.3).

After this, the five best results provide the settings of 3, 7, 24, 28, and 33 (no. in Tab. 5.3), which all lead to 11 or less edges supposedly being steep fronts. On the basis of those cases, ideal basic conditions for extracting steep fronts could be identified: Four of the five cases were obtained using the second approach.[1] In both number 3 and 7 a grid resolution of 1 m and the parameter *mean slope* (MEAN_SL) were used; they only differ in buffer size (1 and 2 m). With numbers 24 and 28, which have a grid resolution and a buffer size of 5 or 10 m, the parameter *maximum slope* (MAX_SL) showed the best results. Hence, it seems that

[1] Which does not necessarily mean that the second approach is better; there are just more possibilities available with different buffer sizes and four different parameters.

No.	Grid. res. [m]	Buffer [m]	Canny thresh	Parameter	Parameter thresh	Total edges	Edges (thresh)	Edges (snow/ice)	Edges confirmed as SF	Case. Fig.
1	1	1	0.0005	DIFF	31.29	3953	172	52		
2	1	1	0.0005	STD	6.48	3953	338	89		
3	**1**	**1**	**0.0005**	**MEAN_SL**	**79.83**	**3953**	**29**	**6**	**5**	**A**
4	1	1	0.0005	MAX_SL	84.77	3953	29	12		
5	1	2	0.0005	DIFF	40.05	3953	133	39		
6	1	2	0.0005	STD	9.16	3953	176	52		
7	**1**	**2**	**0.0005**	**MEAN_SL**	**79.09**	**3953**	**34**	**9**	**8**[a]	**B**
8	1	2	0.0005	MAX_SL	84.77	3953	29	12		
9	1	5	0.0005	DIFF	61.87	3953	98	27		
10	1	5	0.0005	STD	16.06	3953	81	23		
11	1	5	0.0005	MEAN_SL	69.12	3953	381	41		
12	1	5	0.0005	MAX_SL	84.77	3953	34	12		
13	1	10	0.0005	DIFF	76.20	3953	228	45		
14	1	10	0.0005	STD	21.18	3953	126	26		
15	1	10	0.0005	MEAN_SL	59.67	3953	1813	210		
16	1	10	0.0005	MAX_SL	84.77	3953	88	28		
17	2	2	0.0005	DIFF	60.96	5026	60	18		
18	2	2	0.0005	STD	14.76	5026	81	27		
19	2	2	0.0005	MEAN_SL	74.23	5026	56	16		
20	2	2	0.0005	MAX_SL	84.11	5026	31	14		
21	5	5	0.0005	DIFF	96.76	1371	28	12		
22	5	5	0.0005	STD	24.47	1371	35	13		
23	5	5	0.0005	MEAN_SL	61.71	1371	205	43		
24	**5**	**5**	**0.0005**	**MAX_SL**	**80.14**	**1371**	**19**	**7**	**6**	**C**
25	10	10	0.0005	DIFF	106.46	397	40	20		
26	10	10	0.0005	STD	19.79	397	75	37		
27	10	10	0.0005	MEAN_SL	51.12	397	174	62		
28	**10**	**10**	**0.0005**	**MAX_SL**	**74.17**	**397**	**20**	**11**	**6**	**D**
29	25	25	0.0005	DIFF	96.95	75	30	23		
30	25	25	0.0005	STD	29.58	75	32	23		
31	25	25	0.0005	MEAN_SL	51.79	75	34	18		
32	25	25	0.0005	MAX_SL	63.03	75	19	13		
33	**1**	**-**	**0.0022**	**Gradient**	**-**	**-**	**26**	**11**		
34	2	-	0.0030	Gradient	-	-	38	13		
35	5	-	0.0042	Gradient	-	-	47	20		
36	10	-	0.0055	Gradient	-	-	29	14		
37	25	-	0.0088	Gradient	-	-	18	12		

Table 5.3: Number of obtained edges representing potential steep fronts at different basic conditions (grid resolution, parameter, and buffer [optional]). The five best results are highlighted here, four of them are visualised in Figures 5.10 and 5.11 (entries in *No. in Fig.* relate to those figures). Explanation of columns: Numbers in *Canny thresh* (33–37) and *Parameter thresh* (1–32): determined due to the *a priori* visually defined steep fronts; *Total edges*: extracted by Canny method applying approach 2; *Edges (thresh)*: Canny edges detected with *Canny thresh* (33–37) or filtered by *Parameter thresh* (1–32); *Edges (snow/ice)*: *Edges (thresh)* that intersect snow/ice. Parameters: DIFF = range of elevation [m]; STD = standard deviation of elevation [m]; MEAN_SL = mean slope [°]; MAX_SL = maximum slope [°]. [a]Three edges occur at the same steep front (no. 5 in Figure 5.10B).

scale — represented by grid resolution and buffer size — has an influence on the adequate parameter.

In contrast, the result of number 33 was obtained using the first approach. It was derived from the 1 m resolution grid; most of the other grid resolutions are similarly suited since they do not lead to many more edges. Therefore, with this approach, an influence of scale relating to the resulting edges is less marked.

Influence of scale and comparison of approaches

In Figure 5.9 diagrams of the numbers of edges obtained with different basic conditions are illustrated, permitting an overview of (1) the influence of scale and (2) the two different approaches (parameters). A general correlation of the number of the found edges and scale is not always obvious. However, it is notable that the parameter MEAN_SL is very suitable at finer scales — apparent in numbers 3 and 7 — but yields by far the most edges at coarser scales (mainly relating to buffer size, no. 11 and 15). On average, both the parameters *range of elevation* (DIFF) and *standard deviation of elevation* (STD) perform better at finer than at coarser scales. MAX_SL, on the contrary, seems to be quite constant and less dependent of scale; for instance, the buffer sizes 1, 2, and 5 m yield the same (relatively small) amount of edges (11–12). The parameter *gradient*, which was used in the first approach, seems to be rather independent of scale.

Comparison of the two approaches shows that the first appproach provides slightly better results at grid resolutions 2 and 25 m (13 and 12 edges, resp.). In contrast, the second approach seems better at resolutions 1 and 10 m (6 and 11 edges, resp.). However, the differences within these results are minimal and the suitability of an approach can only be assigned to individual scales and not to ranges of scale.

Visual analysis of the found edges

Four of the best five results, which were mentioned above, are discussed in the following as cases A–D and illustrated in Figure 5.10 (A, B) and Figure 5.11 (C, D). Besides the edges representing the *a priori* defined steep fronts (1, 6, 7, and 8), two edges were detected that were subsequently confirmed as steep fronts (L. Fischer, pers. comm.): steep front 4 (detected in C and D) and 5 (detected in all four cases). The remaining found edges (one in cases A, B, and C, and four in D) cannot be defined as steep fronts.

As mentioned above, the edges that do not intersect snow or ice cover were excluded. Within the four discussed cases, at most 25 such edges exist (case B). They naturally occur

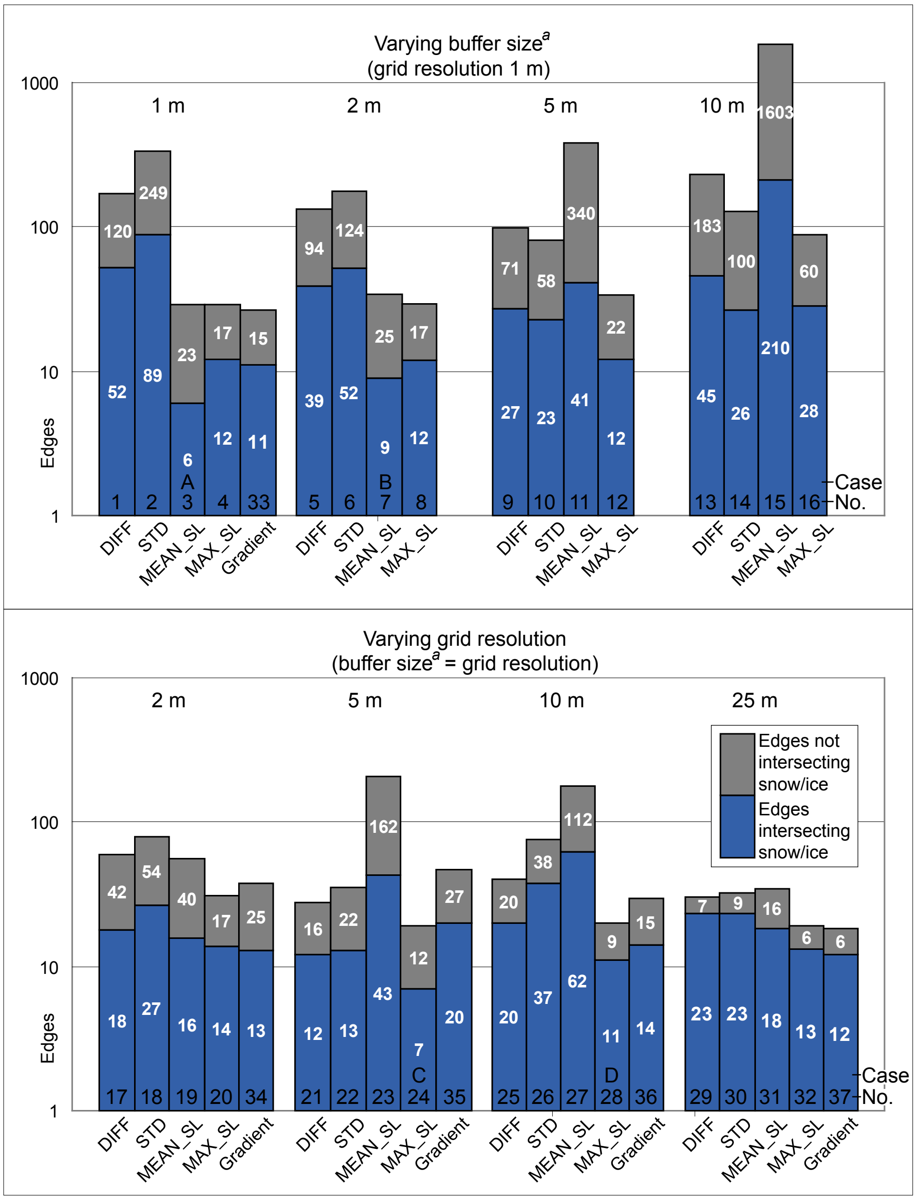

Fig. 5.9: Number of obtained edges representing potential steep fronts at different basic conditions. Entries from Table 5.3 as a bar chart. Bar size indicates the number of edges that were identified given the threshold from the *a priori* marked steep fronts; the lower part corresponds to those that intersect snow/ice, which are supposed to be steep fronts. Basically, the less edges were obtained, the better the basic conditions are. The five best results are numbers 3, 7, 24, 28, and 33; four of them are visualised in Figures 5.10 and 5.11. No. = Number in Table 5.3; Case = label in Figure 5.10 (A,B) and Figure 5.11 (C,D); DIFF = range of elevation; STD = standard deviation of elevation; MEAN_SL = mean slope; MAX_SL = max. slope; Gradient: from Canny edge detection. [a]A buffer was not used with the parameter *gradient*.

in bedrock areas, mainly in the north-western, upper part as well as in the southern part of the face (Fig. 5.10 and Fig. 5.11). Some of them (e.g. those in the upper right area) are oriented in the same way as steep fronts that is to say normal to the cross-sectional plane. In contrast, many of those in the southern part are more oriented to the direction of the maximum slope.

There is one observed exception to the above stated rule that steep fronts intersect snow or ice cover: in A and B (Fig. 5.10) a group of those edges does indicate a steep front (no. 4), which is confirmed within C and D (Fig. 5.11).

Form of the extracted steep fronts

Compared to the visually defined and marked steep fronts, the extracted ones are smaller at finer scales; an extreme example is steep front 5 in case A (Fig. 5.10), where only a very short, hardly visible line developed. At coarser scales, the extracted steep fronts are sometimes longer than the marked ones, with some edges in cases C and D being extreme examples (e.g. steep fronts 7 and 8).

Summary

For best results (that is to say for the identification of the steep fronts that were visually defined) a 1 m grid resolution with a mean slope of 79–80° within a buffer of 1–2 m is proposed. The parameter *gradient* provides almost as good results at 1 m resolution and slightly better outcomes at 2 m. If only lower grid resolutions are available, 5 and 10 m resolutions provide good results using maximum instead of mean slope (approximate thresholds are 80 and 74°, resp.). The parameter *gradient* is the most suitable at 25 m.

On the whole, as shown above, both approaches led to results of similar quality. The first approach provided good and stable numbers through the whole range of scale. The second led to the four best results, however at the cost of the additional zonal analyses. An increase of the buffer size did not lead to a better identification of steep fronts. With the development of this method for the extraction of steep fronts, two new steep fronts were discovered (4 and 5, Fig. 5.10 and 5.11), which had not been identified as such before.

5.2.3 Crevasses

In this section, the results of the extraction of crevasses are presented. Most of the eight *a priori* defined crevasses were identified by the Canny method as edges (Fig. 5.12). Crevasses that show a consistent form in the shaded relief are comparatively well detected

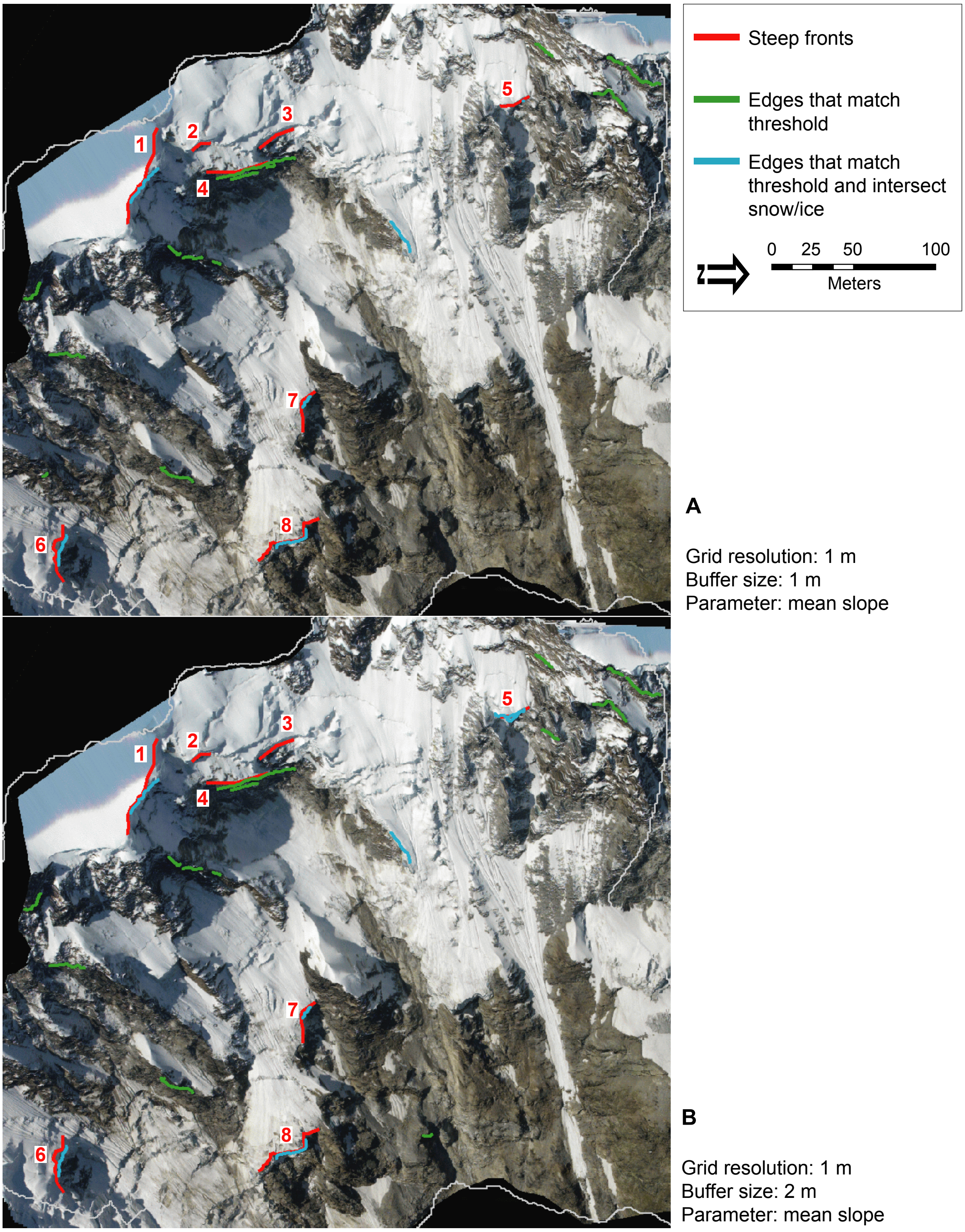

Fig. 5.10: Two of the four best results of the extraction of steep fronts (see Fig. 5.11 for the two others). Steep fronts 1, 6, 7, and 8 were *a priori* defined, while 4 and 5 (represented by four edges) were a posteriori identified by the proposed method as such; 2 and 3 could not be extracted. The white line indicates the extent of the DEM. Orthorectified view.

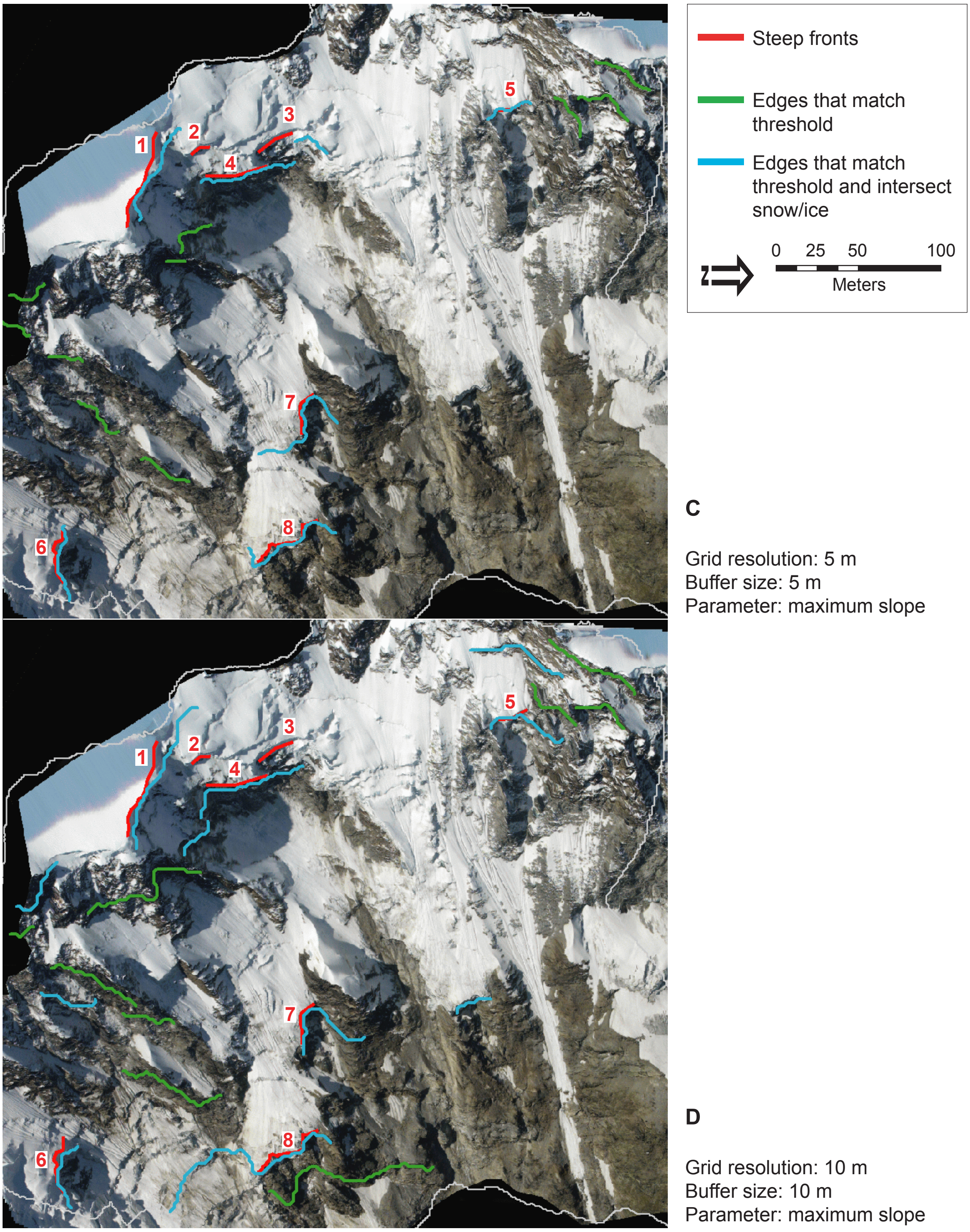

Fig. 5.11: Two of the four best results of the extraction of steep fronts (see Fig. 5.10 for the two others). Steep fronts 1, 6, 7, and 8 were *a priori* defined, while 4 and 5 (represented by four edges) were a posteriori identified by the proposed method as such; 2 and 3 could not be extracted. The white line indicates the extent of the DEM. Orthorectified view.

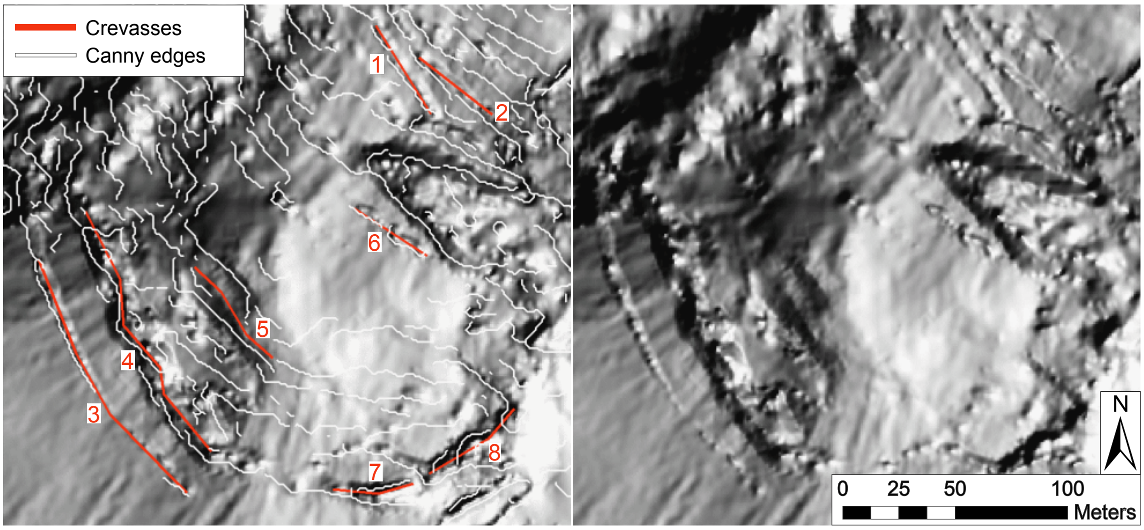

Fig. 5.12: Identification of *a priori* marked crevasses by Canny edge detection (left). The crevasses were marked by means of the shaded relief, which is clearly visible on the right. Extent see quadrangle C in Figure 5.2.

(1 and 7); those that are more irregular (e.g. 4, 6, 8) consist of more, and less parallel, Canny edges. Crevasse 3 was only halfway detected, because the used threshold was too high in order to detect the less clear part of the crevasse. Edges were generated that also originate from higher terrain variations (e.g. steep fronts) and from low terrain variations (glacier surface irregularities; Fig. 5.12). Some edges cannot be traced back to certain surface characteristics; for instance, the many generated edges on the glacier surface between the crevasses 5, 6, 7, and 8 are not visually recognisable. They seem to be artefacts of the edge detection.

In order to distinguish the edges representing crevasses from the others, it was attempted to use parameter thresholds, similar to the extraction of steep fronts. However, it was not possible to find reasonable thresholds of those parameters in order to set the boundary to larger discontinuities (e.g. steep fronts) on the one side, and to smaller irregularities of the snow/ice cover on the other.

5.2.4 Geological planes

For the extraction of geological planes two different approaches were evaluated: (1) division into combined slope/aspect classes according to Brewer and Marlow (1993), and (2) extraction of the morphometric *planar* class according to Wood (1996).

(1) Classification of slope and aspect

The available DEM was classified into 25 combined slope and aspect classes with each class representing a certain aspect azimuth and slope angle (Fig. 5.13). Hereby, planes with similar orientation are denoted with the same colour. The result is illustrated by means of three planes in the middle left of the wall (Fig. 5.13 and 5.15). They could be extracted and were assigned to the same class, namely 31, which represents aspect azimuths 337.5–22.5° and slope angles 45–67.5°. They are surrounded by cells of the class 32, indicating a more eastern aspect azimuth (22.5–67.5°). Aside of those three planes, many more of the same class occur in the wall.

The above stated results basically apply for all evaluated grid resolutions. However, in finer scales, up to 5 m resolution, the planes are not as well developed as in coarser scales; due to more details, they often show pixel islands representing other classes. In contrast, the details are reduced in coarser scale; for instance, with 25 m resolution, the middle plane consists of only three pixels. A good compromise between form and detail for those three planes is provided by the 10 m resolution grid, the result of which is shown in Figures 5.13 and 5.15.

Near thresholds that represent class boundaries, streaking can appear. Small changes in the orientation of planes that have azimuth and slope values near a class boundary can lead to a change of class (e.g. classes 33 and 43 in Fig. 5.15).

(2) Extraction of Wood's morphometric class plane

The best possible basic conditions for the extraction of planes with Wood's method were found to be using the 10 m resolution grid with a 5x5 analysis window size and a curvature tolerance of 0.5 (Fig. 5.14). Still, the three planes, which act as examples, are hardly recognized as being allocated to the class plane, but more to the classes channel and ridge (Fig. 5.15B).

As outlined in section 5.1.1, raising the curvature tolerance leads to an increase of the plane fraction at the cost of the channel and ridge fractions. Hence, those three planes are clearly visible. However, also many non-planar features are recognised as planes in this manner.

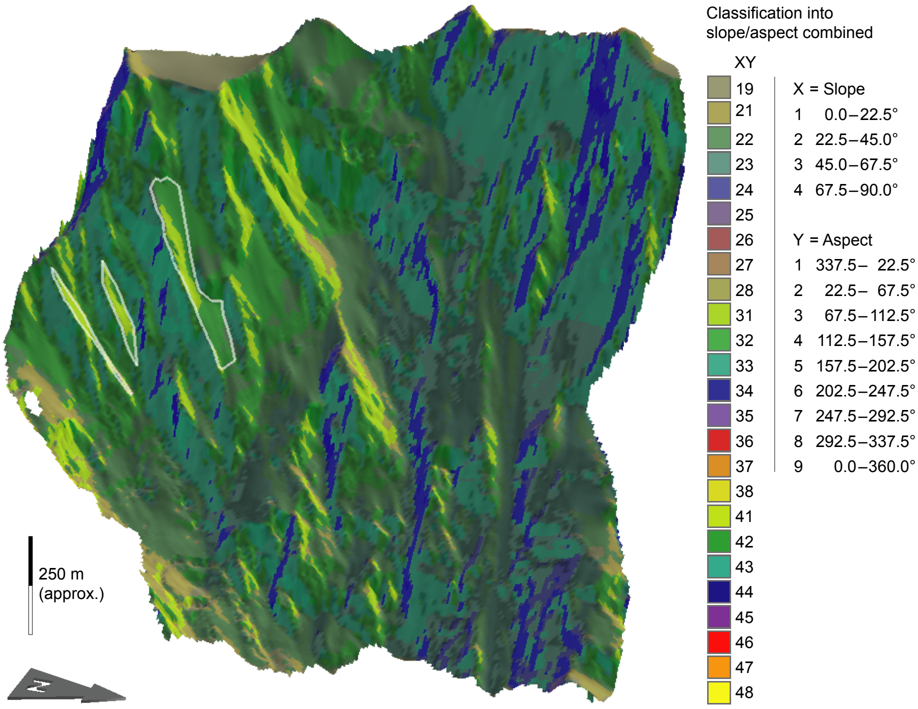

Fig. 5.13: Division of the 10 m DEM into 25 slope/aspect classes analogous to Brewer and Marlow (1993). Detail of the three sample planes (white outlines) see Figure 5.15. Raster is draped over the 10 m DEM.

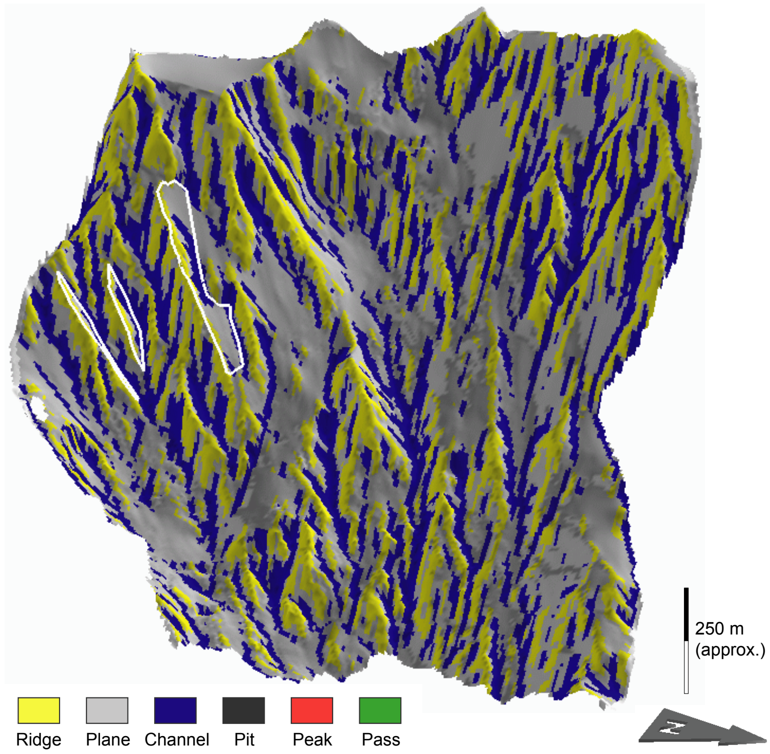

Fig. 5.14: Classification of the 10 m resolution DEM according to Wood (1996).

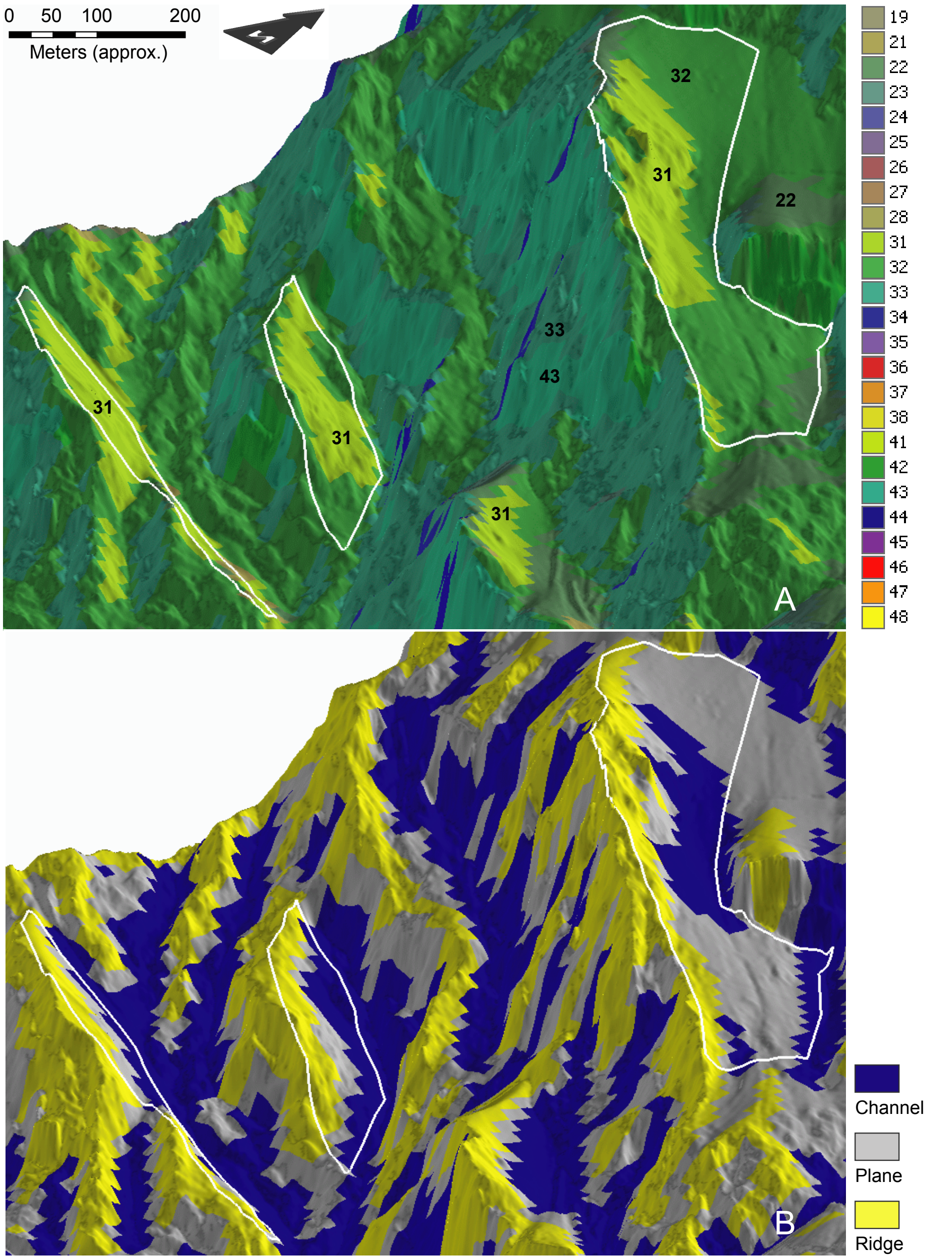

Fig. 5.15: Classification of the 10 m resolution DEM according to Brewer and Marlow (1993, A) and Wood (1996, B). Zoom to the three sample planes (white outline) from Figures 5.13 and 5.14. Perspective is slightly different than in those figures. Class 31 (sample planes) means a slope within 22.5–67.5° and an aspect within 337.5–22.5°; see Figure 5.13 for a detailed description of the legend. The raster grids are draped over the 1 m DEM. Extent see quadrangle B in Figure 5.2.

6 Discussion

In this chapter the results are interpreted and compared to previous research. Important aspects and limitations are pointed out. Confirmation of the aims expressed in section 1.2 and recommendations for future work will be elaborated in the chapter Conclusions.

The structure of this chapter is similar to the previous two chapters. The results of the examination of defined feature extraction methods are discussed in the first section and the extraction of specific features is illuminated in the following section. Finally, fundamental feature extraction aspects such as the division into bottom-up/top-down, the importance of scale, the pixel-based/object-based approaches, and the use of 2.5D versus 3D are discussed.

6.1 Application of specified methods (bottom-up approach)

In the following the results of the application of three specified methods are evaluated. General comments on the bottom-up (and top-down) approaches are given in section 6.3.1

6.1.1 The six morphometric classes by Wood (1996)

The classification of the DEM into the six morphometric classes by Wood (1996) is not a bottom-up approach *sensu stricto*, since the resulting classes or features are basically already known. However, these are very fundamental classes, which may extract different features when applied to different landscapes. Therefore, its application for a high-alpine DEM may reveal an unexpected benefit.

The classification of the DEM by Wood's method led to the identification of the feature types ridge, channel, and plane. The peaks and passes of the Monte Rosa were not classified as such, because the DEM does not continue behind the ridge.[1] Pits do not exist within the wall.

[1]Even with strongly increased slope tolerance and with a large cell size of 25 m most of those peaks and passes are not recognised as such. For instance, the prominent Dufourspitze is clearly identified as ridge instead of peak.

The classification is strongly influenced by scale (grid resolution or analysis window) as well as by the curvature tolerance and the slope tolerance.

Influence of scale

For the investigation of the influence of scale different grid resolutions were considered. Another possibility would have been to adjust the analysis window size (fixed or fuzzy), which would, in principle, have led to similar results. Most importantly, scale determines the level of detail of the extracted features; detailed features such as rills are recognised at finer scales, whereas at coarser scales large rock ridges are identified.

Another effect of scale is the observed change of proportion between the extracted classes ridge, channel, and plane (Table 5.1). From finer to coarser scales the ridge and channel fractions increase at the cost of planar cells. The reason might be that the DEM becomes smoother (in the sense of "wavy" or "curved") with increasing generalisation: the planar regions obtain a higher curvature and are therefore more often recognised as ridges or channels.

Curvature and slope tolerance

If Wood's method is strictly applied, that is to say with zero tolerance values, it will produce mainly channels and ridges, because (1) DEMs rarely show a profile curvature of zero and (2) true peaks, pits, and passes usually have an overall slope (Wood, 1996, p. 117). Thus, the default values in Landserf are slightly greater than zero; they were raised in some examples to observe the implication on the classification (Fig. 5.3).

The increase of curvature tolerance resulted in more planar cells at the cost of ridge and channel cells, because the curvature of a specific cell must be higher in order to count as part of a "curved" feature (e.g. ridge or channel). With a raised curvature tolerance, primarily the snow and ice cover is identified as planar, which can be explained by its smooth surface.

A higher slope tolerance forced the identification of peaks, pits, and passes, although they do not exist within the wall (see above). The reason for this is that a higher overall slope is permitted. Therefore, an increase of the slope tolerance can help point out areas that are close to being related to one of these classes.

Summary

In summary, Wood's classification method can give a fast and rough overview of characteristic features or key areas within a DEM. The suitable basic conditions depend on the needs of the user. By adjusting scale, the level of detail and the proportion of the identified classes can be influenced. The latter can also be accomplished by adjusting the tolerance values.

The application of Wood's method identified many ridges and channels within the Monte Rosa east face, indicating the gravitational processes within the wall. Furthermore, with increased curvature tolerance, the snow and ice cover is emphasized by the planar class, suggesting that this method could be used for the rough identification of the snow/ice cover if auxiliary datasets are not available (cf. sec. 6.2.1).

6.1.2 Application of terrain roughness

The use of the land-surface parameter terrain roughness (Olaya, 2008, p. 158) was investigated as a possible method for feature extraction. The calculation method Vertical Ruggedness Measure (VRM, Sappington et al., 2007), which is based on Hobson (1972), had been proposed as being effectively independent of slope when analysing mountain ranges (Sappington et al., 2007). Within this work, the independence of slope was also confirmed for steep rock faces ($r = 0.38$; Fig. 5.4).

In general, terrain roughness decreases as scale becoming coarser (Fig. 5.5). The inverse correlation between roughness and scale can be traced back to the reduced terrain variability by averaging height values. Only from the 1 m to the 2 m DEM (both calculated with a 3x3 analysis window) the maximum roughness increases (from 0.74 to 0.78), which can be explained by the different interpolation methods that were applied for grid generation (see sec. 4.1.1).

Using this method, however, not only "rough" areas but also edges are measured as rough. This happens because VRM measures roughness by dispersion of the normal vectors of combined slope and aspect (Sappington et al., 2007), automatically leading to high dispersion — and hence high roughness — at distinct edges. In fact, not only small-scale edges such as of boulders are identified as rough (which would be desirable), but also large-scale edges such as steep fronts. This is particularly unwanted at coarser scales, where the large-scale ridges are identified as the roughest areas of the study area (e.g. 25 m, Fig. 5.5). The roughness of edges is also discussed within the context of the extraction the snow and ice cover (sec. 6.2.1).

In order to bypass this problem, either VRM might be adjusted such that edges are not identified as rough, or a roughness might be otherwise measured, for instance by fitting a plane to the cells in the neighbourhood and by subsequent calculation of the standard deviation of the plane (Sakude et al., 1998). However, it is likely that edges are always seen as rough with all measuring methods, because roughness represents terrain variation, which is naturally higher at edges than in planes.

Since terrain roughness indicates how undulating the terrain is, areas of high variation are extracted, which are mainly bedrock in the study area. Therefore, it was attempted to use roughness for the differentiation between the snow/ice cover and rock (sec. 6.2.1).

6.1.3 Application of reflectance intensity

It can be recognised that the snow and ice cover locally has a higher intensity value than rock, because it is brighter and reflects the laser beam (Fig. 5.6). Theoretically, this fact could have been used for differentiation between snow/ice and rock. However, the flight streaks of the acquisition procedure are clearly visible, thus it is hardly possible to make global analyses.

The reason for the streaks is, that intensity is not only dependent on surface reflectance, but also on changing of laser beam divergence, topography, or flying altitude (Höfle and Pfeifer, 2007); radiation, light, and temperature are further important factors. Thus, the intensity data would have to be corrected for further processing. As this is a complex and time-consuming task (cf. Höfle and Pfeifer, 2007) and is in development, it was decided not to consider the reflectance intensity for feature extraction.

In the future the intensity values of the available lidar dataset might be corrected (e.g. according to Höfle and Pfeifer, 2007) in order to use them, for example for glacier surface segmentation, as was done by Höfle et al. (2007).

6.2 Extraction of specific features (top-down approach)

In this section, the results of the extraction of the four previously specified features are evaluated.

6.2.1 Snow and ice cover

Using terrain roughness, the snow and ice cover was identified with a maximum accuracy of 70 % (Table 5.2). This means that 70 % of all cells were correctly identified as snow/ice or rock, on the basis of the snow/ice vector layer, which was manually digitised from the orthophoto. Since the maximum accuracy is similar at all evaluated scales, this method seems to be rather independent of scale.

The rather frequent incorrect identification of snow/ice as rock is the main reason why the maximum accuracy does not exceed 70 % (Table 5.2). This arises from the fact that edges are always seen as rough (sec. 6.1.2), also those within the snow/ice cover (mainly steep fronts and irregularities in the snow and ice cover). Using a multi-scale representation of roughness (Fig. 5.8), the roughness of bedrock edges and of snow/ice edges at different scales was compared. This showed that both edge types are seen as rough at all scales. Hence, snow/ice edges cannot be isolated in order to improve the accuracy of the method.

Besides the low identification accuracy, the following limitations must be considered:

1. *Scale-dependency:* The roughness threshold is different for each scale (0.001, 0.02, 0.004; Table 5.2). Here, the optimal thresholds for three different scales were iteratively determined (three different combinations of grid resolution and scale). For other scales the roughness threshold is not known. It seems that there is a positive correlation between cell size (scale) and threshold, which makes sense because the increase in cell size involves smoothing. At coarser scales a cell therefore needs a higher roughness value in order to be identified as rock.

2. *Transferability:* the determined roughness thresholds might not apply for other regions and datasets, due to different basic conditions.

3. *Control dataset:* the achieved maximum accuracy is not only dependent on the extraction method and on scale, but also on the control dataset represented by the snow/ice vector layer, which was manually digitized from the orthophoto. A more accurate control dataset might have led to different (better or worse) extraction accuracy.

For all its limitations, terrain roughness is an obvious tool for the differentiation of snow/ice and rock, since rock is commonly rougher than the surface of snow and ice. However, according to the knowledge of the author, snow and ice cover has not been extracted solely from a DEM to date. It is much more common to extract snow and ice from aerial and satellite imagery (e.g. Srivastava and Stroeve, 2003; Venkataraman et al., 2008). If such images are not available, terrain roughness might come into consideration for a rough identification of snow and ice.

For further work a different approach for roughness measurement might be found that does not identify edges as rough and hence provides a more accurate identification of the snow and ice cover.

6.2.2 Steep fronts

It was attempted to find a method to extract steep fronts from the available DEM. Overall, eight steep fronts were visually identified within the DEM perimeter. At suitable basic conditions (no. 24 in Table 5.3) seven edges could be extracted, six of which were actually validated as being steep fronts (Fig. 5.11C). The remaining edge cannot be denoted as steep front (north of steep front no. 3).

Despite this rather good result, it is difficult to make a recommendation for the extraction of steep fronts. Quite different basic conditions from the ones mentioned above did lead to similar results, whereas some similar basic conditions lead to very different outcomes. As it is not easy to recognise an overall pattern within the results, some notable aspects of the method and of the results will be discussed in the following.

Approaches to extract edges and Canny edge detection

As shown in Figure 4.4, two different approaches were applied. The first uses Canny edge detection for the filtering of the edges, the second zonal analysis. Both approaches use Canny edge detection initially. Compared to other edge detection methods such as Sobel and Prewitt, the main advantages of the algorithm by Canny (1986) are exact positioning as well as connected and distinct lines (Zhou et al., 2008). For these reasons this algorithm is now widely used in edge detection (Li-chun, 2002; Zhou et al., 2008). A disadvantage of the algorithm is that only two of three edges that meet in one point can be connected. However, this did not concern the present work.

The edge detection threshold not only affects whether an edge is detected, but also how long the edge is. When different thresholds were used, the two approaches provided steep fronts of different lengths. Thus, all detected edges using the first approach are generally shorter, since the threshold is always greater than 0.0005 ($\geq$ 0022, no. 33 in Table 5.3). As an example, the obtained edges at the steep fronts 7 (Fig. 5.11C) and 8 (Fig. 5.11D) are longer than the actual steep fronts and even cross the rather flat glacier, although no strong height variation exists. The reason for those overlong edges is that the low threshold of 0.0005 was used. Therefore, the calculated gradient values seem to have been between the two (high and low) Canny thresholds and edge following occurred over the glacier surface. With the first approach, the threshold is much higher at these grid resolutions (no. 35 and 36 in Table 5.3), leading to edge lengths that better represent the steep fronts, probably because the mere detection and the length of an edge correlate. The second approach does not seem to be suitable at coarser scales to detect an appropriate edge length, because detection and length are decoupled, and the "existence" of an edge is not decided by the detection threshold but by zonal analysis.

Parameters and scale

The thresholds of the parameters *range*, *standard deviation*, and *gradient* increase with scale becoming coarse (Table 5.3; Fig. 5.9). This can be explained by the fact that with increasing buffer size the range of values and hence the standard deviation increases, and consequently the threshold value has to be raised. In contrast, the thresholds of the parameters *mean slope* and *maximum slope* decrease with increasing scale. This is due to the fact that the DEM becomes smoother with coarsening scale through interpolation, and the slope values are hence lowered by averaging the elevation values. Maximum slope behaves specially with increasing buffer size: it does not change, because the highest slope value remains the highest even at larger buffer sizes.

Relating to the least number of detected edges, where the four defined steep fronts are still included, it can be said that of all parameters *maximum slope* provides the best results at almost all scales (cell sizes and buffer sizes). This might be explained by the fact that this parameter best represents the character of steep fronts, which is their very high slope. Mean slope is similarly suitable at finer scales, but gives inferior results at most coarser scales. This can be ascribed to the fact that the mean slope strongly decreases with increasing buffer size; similarly, at larger cell sizes, the mean slope is diminished by the smooth surface deriving from grid interpolation. Both parameters *range* and *standard deviation* provide similar results, showing that they correlate. However, they are always less suitable than maximum slope. A possible explanation for this is that both these parameters are less characteristic of steep fronts than the maximum slope, because a steep front does not necessarily need to be particularly high, but naturally has a very high slope.

At a fixed Canny detection threshold, the number of detected edges is considerably influenced by scale (cell size; Table 5.3). Numbers range from 75 (25 m cell size) up to 5026 (2 m cell size). There seems to be a negative correlation between scale and edge quantity. This can be explained by the averaging of height values through interpolation to larger cells: the variation of height values decreases and the calculated gradient is often below the detection threshold. According to this it was expected that the 1 m grid would lead to the greatest number of edges, which it does not. This might be explained by the different interpolation methods used (sec. 4.1.1). Therefore, the production process of the DEM can have a significant impact on the result of feature extraction.

Edge length and scale

As mentioned above, edge length varies with the Canny edge detection threshold. It was concluded that the first approach provides more suitable edge lengths than the second. This holds particularly true for cell sizes from 5 m on, where some edges cross flat areas. At finer scales, the edge lengths from the second approach are also useful: at 1 m resolution the detected edges are shorter than in reality (Fig. 5.10) and at 2 m resolution they represent the steep fronts best.

The reason for the observed fact that edge length increases with cell size is similar to the one explained above concerning the number of edges. By averaging the height values through interpolation to larger cells, the height variations decrease, whereby the edge following of the Canny algorithm is less constrained, resulting in long and "weak" edges.

Buffer size

The evaluation of buffer sizes at a fixed resolution showed that increasing buffer size leads to worse results (too many edges that do not represent steep fronts). This can be explained by the relatively low horizontal extent compared to the vertical extent of a steep front; a larger buffer comprises more areas that do not actually belong to the steep front. The effect of a too large buffer is particularly pronounced for the parameter *mean slope*. Since the slope of a large buffer area is averaged, it cannot be used as filter parameter anymore because it does not represent the high elevation variation within a small area anymore. Consequently it was assumed that the most appropriate buffer size corresponds to the grid resolution; this understanding was then applied to the other resolutions.

Intersection with snow/ice

As many previously detected edges appear within rock and therefore do not represent steep fronts by definition, the results were filtered by intersection with the snow and ice cover. This operation led to a reduction in the number of edges from only $\sim$23 % (no. 29, Fig. 5.9) to $\sim$88 % (no. 15), depending on the basic condition. In general, this operation has a stronger effect, that is to say filters more edges at finer scales (cell sizes) than at coarser scales (Fig. 5.9). This can be explained by the detected edges being shorter and appearing more frequently in rock than in snow/ice due to the higher variation of the terrain, particularly in rocky areas; in contrast, at coarser scales, the detected edges are longer and hence more probable to intersect the snow/ice cover.

The intersection of the edges with the snow and ice cover provided useful results where edges represent almost only steep fronts and almost all known steep fronts were extracted (e.g. no. 3, 7, 24, and 28).

Limitations

Although Canny edge detection, filtering with thresholds, and the intersection with the snow/ice cover led to suitable results, there are some limitations that must be considered when using this method:

1. The determined thresholds are very unstable. Their adjustment can lead to rapid changes in the number of obtained edges. For that reason the determined thresholds cannot be blindly transferred to another dataset; a visual control and an iterative adjustment will probably be necessary.

2. As the length of edges depends on two factors — grid resolution and edge detection threshold — it is hard to control it. Filtering the edges by edge detection threshold instead of zonal analysis seems to lead to more realistic lengths, which might be explained by the fact that the threshold controls both (1) if an edge is detected, and (2) how long it is, whereas, for zonal analysis, a relatively low threshold has to be chosen, eventually leading to overlong, unrealistic edges/steep fronts.

3. A dataset containing the snow and ice cover has to be available. Otherwise, many edges representing rock ridges remain in the result.

Summary and outlook

Steep fronts play an important role in the context of natural hazards. Therefore it was attempted to develop a method to automatically extract them from a DEM. As this was not possible, the available orthophoto was used as an aid. With optimal basic conditions, the false positives and misses were reduced: by choosing thresholds as high as possible, edges that do not represent steep fronts (false positives) were minimised. The steep fronts that were not detected (misses) were reduced by selecting four typical steep fronts for determining the minimum threshold.

Overall, the use of Canny edge detection according to the first approach applying the determined gradient thresholds (no. 33–37 in Table 5.3) and subsequent intersecting with the snow/ice cover may lead to satisfying results regarding the detection and length of the edges. Zonal analysis (second approach) is much more laborious and does not provide significantly better outcomes.

For future work, the determined parameters and thresholds could be evaluated for other glaciated rock faces. A possible way for improvement might be to use an object-oriented approach instead of a pixel-oriented one (see sec. 6.3.3).

6.2.3 Crevasses

It was possible to identify most of the previously observed sample crevasses using Canny edge detection (Fig. 5.12), however no way was found to distinguish those edges representing crevasses from those representing other features such as steep fronts or glacier surface irregularities, or from artefacts. Whereas steep fronts could mostly be distinguished from other features using the same approach, this does not hold true for crevasses. The main reason for this lies in the nature of crevasses: they are not features that are clearly defined by a certain attribute — whereas steep fronts can be identified by very high slope values. In fact, crevasses lie between very coarse-scale (steep fronts) and fine-scale elevation variations (smaller snow/ice cover irregularities), therefore two thresholds would have to be identified for the extraction (in contrast to steep fronts, where only one threshold had to be determined).

Furthermore, the edge detection did not provide as qualitatively good edges as it did for the identification of steep fronts. Thus, a crevasse is often represented by many lines that are not connected, and which are also often oblique to one another. The reason for this might be that the crevasses are rather irregular (no. 4, 6, and 8 in Fig. 5.12) or are not distinct in the DEM (no. 2). Artefacts arising from the interpolation of the lidar data might also be involved; sometimes the crevasses seem to be partly closed by interpolation or seem to show a bull's eye pattern (1, 2).

Many edges were generated that do not seem to reflect the glacier surface. It is not visually recognisable, if they represent real small-scale variations of the surface, or artefacts that arise from edge detection due to the very low threshold. If a higher threshold had been chosen, fewer of the assumed artefacts would have emerged, but crevasse 3 would not have been detected (even with the applied threshold, it is only half-way detected).

In summary, the following represent notable limitations in using this method for the extraction of crevasses:

1. Although the Canny edge detection method does detect most crevasses using a rather low threshold value, the detected lines are often not connected and oblique to each other.

2. Those detected edges representing crevasses can hardly be separated from other fea-

tures such as (coarse-scale) steep fronts, (fine-scale) surface irregularities, as well as from the assumed artefacts.

3. An auxiliary dataset representing the snow and ice cover must be available, in order to obtain those edges that are supposedly crevasses. This limitation is the same as in the extraction of steep fronts.

Höfle et al. (2007) applied a different approach to detect crevasses. They used a combination of reflectance intensity and terrain roughness to segment the lidar point cloud of the glacier surface into the target classes ice, firn, snow, and surface irregularities, with the latter mainly comprising crevasses. Although they could not extract discrete features representing crevasses, their approach seems to be more successful in the identification of crevasses.

For future work, since the crevasses are sometimes not well represented by the available 1 m resolution, a more detailed DEM might be more suitable to represent those fine-scale features and for their identification by edge detection. However, this will also lead to a higher variability and "noise", which again diminishes the generation of connected lines. For all the above mentioned reasons, edge detection does not seem an appropriate method to extract crevasses from a DEM. A more object-oriented, model-driven approach, as the one by Höfle et al. (2007) might lead to more promising results, although it is not known whether glacier and bedrock irregularities can be differentiated.

At least, Canny edge detection could be interesting for the identification of glacier surface irregularities in general. However, a higher threshold would have to be chosen in order to prevent the generation of meaningless edges (artefacts).

6.2.4 Geological planes

As geological or geomorphological planes can give a good understanding of slope instabilities, a method for the extraction of those planes was sought. The classification method by Brewer and Marlow (1993), which divides a DEM into 25 classes combining slope and aspect values, was found to be suitable (Fig. 5.13, 5.15). The most suitable grid resolution for the three defined target planes is 10 m; a higher resolution leads to planes comprising islands representing other slope angles and directions; a lower resolution results in less detailed planes.

With this method, within the whole Monte Rosa east face, planes of the same joint system could easily be recognised Fischer (2006). The big advantage is that the approximate slope and aspect is assigned to each planar object. According to this, the main jointing dips 45–67.5° to 337.5–67.5° (classes 31 and 32). A further distinct set of planes shows the same dip range (45–67.5°) but with a more south-easterly aspect (67.5–157.5°; classes 33 and 34).

Comparison between methods by Brewer and Marlow (1993) and Wood (1996)

In contrast, the second tested method (Wood, 1996) could not extract such distinct planes as the three defined ones (Fig. 5.14, 5.15); instead of being assigned to the morphometric class plane as expected, they were assigned to the classes ridge and channel with different basic conditions. Although a higher curvature tolerance would lead to more cells being classified as planar, not necessarily plane (flat) objects but rather smooth (that is to say *not rough*) areas would have been considered.

The difference between the two proposed methods can be explained by their essentially different approaches. The classification by Brewer and Marlow (1993) is based on first derivative parameters, Wood's on second derivative parameters. The three sample planes show specific orientations but their surface is not necessarily plane but rather rough. This might be the reason why they are not identified as planar by Wood's approach, which seems to be more adequate to identify "smooth" regions.

Previous research

Jaboyedoff et al. (2004) applied a similar method for the representation of a DEM and developed the software Coltop-3D, which displays the orientation of a pixel of a DEM using a Hue-Intensity-Saturation coding in a stereographic projection. Here, too, both slope and aspect are coded in one colour. Derron et al. (2005) used this method for the determination of the orientations of discontinuities as a preparation for preliminary assessment of rockslide and rockfall hazards.

The approach by Brewer and Marlow (1993) resembles this method since slope and aspect are represented in combination. However, it differs in that the pixel values are combined into classes, reducing the number of colours. The advantage of having classes is that discrete objects (represented by the classes) are obtained. They represent similar pixel values, or, to put it in another way, areas of similar slope and aspect. Brewer and Marlow (1993) divided the values into 25 classes, which seems to be a reasonable compromise between the appearance or dimension of the detected planes and their homogeneity.

Significance

The method by Brewer and Marlow (1993) is a simple and yet valuable tool for the extraction of planes. If a suitable cell size is used, the planes are rather homogeneous and hardly contain "islands" of other classes, that is to say other slope and aspect values. A particular advantage is that the classes are coded in such a way that the slope and aspect values can easily be recognised. In contrast to methods that use curvature in order to extract planar objects (e.g. Wood, 1996), this method can also identify planes, the surface of which is not necessarily smooth, but can also be irregular, rough, or partly covered with snow. If more or fewer classes are necessary, the method can easily be adapted by adjusting the mapping values. Since this method is not dependent on thresholds, it can be very well transferred to other study areas.

Limitations

A disadvantage of the classification method is the streaking that can appear with planes showing slope or aspect values near class boundaries. Thus, small changes in the orientation of planes near a class boundary can lead to a change of class, in extreme cases even in an alternating pattern. This phenomenon is dependent on the number of classes: the more classes the DEM is divided into, the more probable the appearance of streaking becomes. However, a reduction of the class number would lead to a less distinct identification of planes. A further limitation concerns the visualisation of the classes, for which the colours proposed by Brewer and Marlow (1993) were applied within this work. It must be considered that this colour selection assigns brighter colours to steeper planes and highlights these.

Improvements

As with the other covered feature extraction methods, a better result might be achieved by a more object-oriented approach. However, a difficulty would be planes with an irregular surface.

6.3 Overall aspects of feature extraction

In this section, overarching aspects that concern all above treated feature extraction methods are discussed.

6.3.1 Bottom-up and top-down approach

Within this work, two different approaches for feature extraction from the available DEM were evaluated, bottom-up and top-down. Bottom-up means that an initially specified method is applied and tested for its suitability (Table 6.1). It is not necessarily known from the beginning, which features will be extracted. This approach was used to find out what certain methods can contribute to feature extraction from an alpine rock wall.

The method by Wood (1996) does not represent a strict bottom-up approach, because it is known from the beginning which classes or features the DEM will be divided into. Yet this method was denoted as a bottom-up approach within this work, because the goal was not to detect those six features classes in the first place, but to find out, if Wood's method is also suitable for an alpine rock wall, and, if more typical or specific features can be identified.

Primarily, terrain roughness was used as a classic bottom-up approach. Its evaluation showed that it appeared to be suitable for the distinction of different surface textures and types in general. Specifically, it may be used for the differentiation between the snow/ice cover and bedrock. As snow/ice had been specified as target feature, terrain roughness was evaluated as a possible means to extract snow/ice, and was therefore used as a both bottom-up and top-down approach.

The use of reflectance intensity can also be called a classic bottom-up approach; however it could not be evaluated due to data inhomogeneity.

With a top-down approach, it is attempted to find a suitable method for the extraction of initially specified features. This represents a more practical approach since specific features that are of known interest are to be evaluated.

At first glance the top-down approach might seem more goal-oriented than the bottom-up approach. However, both have their justification and can provide significant results. If specific methods (e.g. Wood's) or parameters (e.g. terrain roughness) have not been used for a certain kind of study area, or, if certain attributes (reflectance intensity) are available for analysis of the study area, it is important to evaluate their suitability. For instance, the bottom-up approach terrain roughness turned out to be an adequate means for the extraction of a previously specified feature (snow/ice cover).

Other use of bottom-up and top-down

Within this work, bottom-up and top-down describe whether a method or a feature type is initially specified for evaluation or extraction, respectively. Straumann and Purves (2008) used these terms in a similar way, insofar as they denote top-down as starting with the

Section	Approach	Method	Target feature	Most suitable scale [m][e]	Feature size (appr.) [m]
x.1.1	Bottom-up	**Six morphometric classes**[a]	(not specified)	?	-
x.1.2	Bottom-up	**Terrain roughness**[b]	(not specified)	?	-
x.1.3	Bottom-up	**Reflectance intensity**	(not specified)	?	-
x.2.1	Top-down	Terrain roughness[b]	**Snow and ice cover**	1–25	L/W: 40-1000
x.2.2	Top-down	Edge detection[c] a.o.	**Steep fronts**	2–10	L: 100-300, W: 10–50
x.2.3	Top-down	Edge detection[c] a.o.	**Crevasses**	1 (?)	L: 50–150, W: <1-20
x.2.4	Top-down	Combined aspect/slope[d]	**Planes**	10	L: 150–500, W: 10–50

Table 6.1: Overview of the applied methods, the extracted features, and the most suitable scales or scale ranges. Section: x = chapter 5 or 6. Feature size: L = length, W = width. [a]Wood (1996). [b]Sappington et al. (2007). [c]Canny (1986). [d]Brewer and Marlow (1993). [e]Cell size.

notion of a landform and subsequently applying delineating methods. Only the usage of the term bottom-up is slightly different. Whereas it denotes more the strategy aspect within this work, they use it as an approach “in the case of a field-based view of landforms”, where methods are applied to identify areas with similar values of certain attributes. Still, in both views, bottom-up lastly denotes the use of a certain technique to obtain features of similar characteristics, without an initial specification.

Straumann and Purves (2008) use bottom-up in the context of pixel-based and top-down in the context of object-based methods (cf. sec. 6.3.3).

6.3.2 The influence of scale

It is widely recognised that, in order to analyse a DEM, a multi-scale approach is necessary (e.g. Wood, 1996; Schmidt and Andrew, 2005). Therefore, different scales were applied when extracting the four feature types. For each of these, the most appropriate scale or scale range was determined (Table 6.1), which is recommended by MacMillan and Shary (2008). Below, it is attempted to connect the determined scales with the extent of the features. Then, the results of these evaluations are set in context to each other.

Scale and feature size

Within the bottom-up approaches no target features are specified (Table 6.1). Therefore, it is not possible to state the most suitable scale, since this is dependent on the dimension of the target feature. Conversely, within the top-down approach, the most suitable scales for the target features could be determined approximately. It is suggested that there is some correlation between feature size and the most suitable scale for extraction, which will be discussed in the following.

The smallest of all extracted features are crevasses. According to Figure 5.12 their minimum width can be 1 m or possibly even less (e.g. no. 3). At a coarser scale (larger cell size) the smaller crevasses might not be detected in the DEM. Therefore the most adequate scale for their extraction is 1 m or less.

Regarding both length and width, steep fronts are larger in size than crevasses and actually have a higher appropriate extraction size. Whereas the steep fronts could be detected in all scales, their length is only realistic in the range 2–10 m. Thus, scale seems to play an important role relating to edge length when applying Canny edge detection.

The geological/geomorphological planes have a similar dimension to steep fronts and also show a similar suitable scale (range). Since the narrowest plane of interest might be about 10 m wide, it will be hardly recognised at a larger cell size (25 m). The snow/ice cover shows the largest features (areas) and accordingly can also be detected at more than 10 m cell size. Interestingly, the extraction quality is similar at lower cells sizes down to 1 m.

Overall, the suggested correlation between the size of a feature and the suitable scale for the extract extraction can be reproduced. The minimum width of a feature (e.g. crevasse or plane) approximately specifies the maximum cell size for extraction; at a larger cell size it would not be detected. In some cases the cell size may be much smaller (e.g. snow/ice cover or steep fronts). However, a too small cell size can prevent features from being distinctively detected due to “noise” (e.g. extraction of planes).

Scale-free edges

The parameter terrain roughness was calculated at four scales (Fig. 5.8). The outcome shows that edges are seen as rough at all evaluated scales. Therefore the extraction of edges might be scale-free (Shary et al., 2002), that is to say that the edges are invariant and can be recognised regardless of scale.

Comparison with other research

The above findings and interpretations confirm most of the widely accepted opinions. MacMillan and Shary (2008, p. 231) found that the classification of a specific feature relates to a particular range or narrow range of scale, which holds true for most outcomes within this work (at most, the scale range of the snow/ice extraction might be larger than only "narrow".)

According to Evans et al. (2008, p. 520), feature extraction often needs to be adapted to the working scale, or else it might lead to poor results. Within this work feature extraction was adjusted to specific scales by choosing the corresponding cell size. Another possibility is to adjust the analysis window size, possibly using fuzzy membership (Wood, 1996).

When evaluating different cell sizes within this work, as a proxy of scale, it was shown that their adjustment has a significant effect on surface parameters such as slope, aspect, curvature, and terrain roughness. This effect is supported by the findings of Shary et al. (2002). These authors furthermore claim that second derivatives (curvatures) are more sensitive than first derivatives (slope and aspect). This could not be reproduced in the present work.

6.3.3 Pixel-based and object-based feature extraction

Feature extraction methods can be principally divided into pixel-based and object-based approaches. With pixel-based methods, the pixels are classified according to one or more parameters and are then grouped based on the parameter values. With object-based approaches, segments are first built according to a defined pattern, and then classified in a second step (e.g. Wang et al., 2004).

Below, the extraction of the four feature types is brought into context with the pixel-based and object-based approaches. Since the applied methods for extracting areas and linear features are fundamentally different, they are treated separately.

Area features

The area features were obtained using classic pixel-based classification. At first, the pixels were classified due to one or more parameters (terrain roughness for the snow/ice cover, slope and aspect for geological planes) and were then grouped together based on pixel value thresholds. With both feature types, the target classes were known. Such, in snow/ice extraction obviously the two classes snow/ice and rock are distinguished. For the identification of planes, the DEM was divided into 25 classes defined by Brewer and Marlow (1993).

A difference between those two feature types is that the class boundaries are known in only one of the two types. For the extraction of the snow/ice cover, the suitable threshold distinguishing the two classes *snow/ice* and *rock* had to be determined; this threshold is even different at each scale (Table 5.2). Since the classes are known but the boundary is not exactly defined when extracting the snow/ice cover, this approach is called supervised classification (Hengl and MacMillan, 2008, p. 450). Such, training pixels had to be collected in order to decide, from which roughness threshold on snow/ice is identified as such. This was done by comparing the outcome of the classification to a control dataset. Conversely, when extracting the planes, the class boundaries (thresholds) were known, since they are defined by Brewer and Marlow (1993).

As seen in the discussion of the extraction of planes (sec. 6.2.4), the cell size had to be adapted to the dimension of the target planes in order to obtain discrete objects with without within-field variation ("islands"). This problem particularly occurs with pixel-based methods, when the object of interest is considerably larger than the cell size (Carleer et al., 2005). Instead of adjusting the scale to the object of interest, an object-based approach could be considered. This would require to aggregate pixels into groups according to user-defined rules of homogeneity (Dragut and Blaschke, 2006). This can be achieved by image segmentation techniques such as region growing (e.g. Straumann and Purves, 2008) or the method developed by Baatz and Schäpe (2000). However it could be difficult to find appropriate segmentation criteria for the extraction of planes that are undulating and/or partly covered by snow/ice.

For the extraction of the snow and ice cover a more object-based approach could be applied in future work. Region growing could be applied with pre-defined snow/ice pixels being the seed. These pixels could be obtained by multi-scale measuring of terrain roughness (pixels, that are never rough; cf. Fig. 5.8) . However, figuring out appropriate region growing criteria could be difficult, particularly due to surface irregularities such as crevasses. An example for object-based glacier surface analysis is provided by Höfle et al. (2007).

Line features

For the attempted extraction of line features (steep fronts and crevasses), edge detection was used. Edge detection algorithms are pixel-based since they calculate the local gradient magnitude. Based on a given threshold it is then decided, it the gradient indicates an edge. The main advantage of the Canny edge detector (Canny, 1986) is that it can connect detected line segments.

Thus, there seems to be an analogy to the region growing algorithm, where it is decided based on a given criterion, if a neighbouring pixel is added. However, unlike with region growing, no seed pixels can be defined with Canny edge detection. Hence, this approach is not object-based, since it is not possible to define objects at first.

The detection of steep fronts was controlled by adjusting the edge detection threshold.[2] Hence, this approach falls into the category of supervised classification since it divides the DEM into the known classes *edge* and *not edge*, whereas the class boundary or threshold is not previously known (Hengl and MacMillan, 2008, p. 450). The threshold was determined by visual comparison.

In literature, the extraction of linear elements is not brought into context with the term *object-based approach*. It seems that this is used especially in the extraction of regions or segments. However, it might be interesting to develop an object-oriented edge detection algorithm that can be configured by seeds and by defined "line growing" criteria, e.g. for the extraction of steep fronts or crevasses. This would be analogous to the concept of region growing for areal features.

6.3.4 2.5D versus 3D

Within this study, all applied methods use a 2.5D instead of a "real" 3D approach. In 2.5D each cell is assigned exactly one elevation value, whereas in 3D, either more than one height value can be held per cell, or the original point cloud (without grid interpolation) is used. The main reasons for the choice of 2.5D are that it is very common and that the calculations are more convenient to apply. This holds true for gridded DEMs in general (Evans, 1972; Hengl and Evans, 2008). The disadvantage of 3D using more than one height value is that the common analysis algorithms would have to be adapted. A disadvantage of 3D using the original point cloud is that the laser streaks are visible, which are removed by interpolation to a grid with a certain minimum cell size, and that the influence of scale cannot be investigated as easily as with a grid (resolution, cell size).

According to the knowledge of the author, the application of more than one elevation value per cell is not common. The use of the original point cloud, however, has already been conducted in terrain analysis. For instance, Höfle et al. (2007) used the point cloud for glacier surface segmentation. The main advantage of using the point cloud is that topography is not under- or over-sampled (Hengl and Evans, 2008, see also p. 3). A 3D approach may be especially appealing for an alpine rock face, particularly for the extraction

[2]Since the other line feature type, crevasse, could not be satisfactorily extracted, it is not discussed within this section.

of overhanging areas. However, a 3D approach was not applied due to the above named disadvantages.

7 Conclusions

In the first part of this chapter, the research aims and objectives stated in the introduction are re-evaluated. In section 7.2, general conclusions concerning all applied feature extraction methods are given. In the last section, 7.3, suggestions are given as to topics that future research should focus on.

7.1 Re-evaluation of research aims and objectives

1. To find appropriate methods for the automated extraction of features from a partly glaciated rock wall, with the features being relevant to the on-going natural hazard processes. Such features are: (1) the snow and ice cover, (2) steep fronts, (3) crevasses, and (4) geological planes.

(1) Snow and ice cover Large parts of the Monte Rosa east face are covered by steep hanging glaciers and firn/ice fields (Fischer et al., 2006). In recent decades, rapid changes in surface cover such as mainly ablation but also accumulation of ice have been observed (Fischer et al., submitted). Therefore it may be useful for certain applications to automatically detect the snow/ice cover. Although it is common to extract snow/ice from aerial and satellite imagery (e.g. Srivastava and Stroeve, 2003), it may be necessary and/or useful in some cases to detect snow/ice from a DEM alone.

With Vector Ruggedness Measure (VRM; Sappington et al., 2007) the snow/ice cover could be detected from the available DEM with an accuracy of about 70 %. Therefore, this method is suitable for a rough automated identification of snow and ice cover, if auxiliary datasets such as orthophoto, satellite image, or reflectance intensity are not available. However, the derived thresholds may not be transferable to other study sites.

(2) Steep fronts Within this work, a steep front was defined as the margin of an avalanching glacier (or more specifically, hanging glacier), where the slope of the bedrock significantly increases at the glacier margin (sec. 3.1.2). Steep fronts may be the source area of ice avalanches (Pralong and Funk, 2006, p. 33), therefore it is important to detect them within the investigation of an alpine flank.

Most steep fronts of the Monte Rosa east face could be automatically extracted as discrete lines using Canny edge detection (Canny, 1986) and subsequent intersection with the snow/ice cover. They could not be extracted from the DEM alone, because many rock ridges were spuriously identified by edge detection. Therefore filtering by intersection with the snow/ice cover from the orthophoto was necessary. However, as in the detection of the snow/ice cover, the evaluated thresholds may not be transferable to other areas of interest.

(3) Crevasses Crevasses can represent the origin of a destabilisation of large ice masses. For instance, the presence of a crevasse at the front of a terrace glacier (wedge fracture type) is a good indicator of potential danger (Pralong and Funk, 2006, p. 46). Therefore, their identification is necessary in hazard-related analysis.

This work showed that, contrary to steep fronts, it is very difficult to automatically extract crevasses from a DEM using Canny edge detection and an orthophoto as auxiliary dataset. In fact, the crevasses are identified through edge detection, but so are other glacier surface irregularities and assumed artefacts from which the crevasses could not be distinguished.

(4) Geological planes The geotechnical and geometrical characteristics of planes and discontinuities strongly affect the response of steep bedrock to glacier retreat (Fischer et al., submitted). For instance, a rock avalanche can be (part of) a consequence of the surface-parallel setting of rock discontinuities. Therefore, the identification of such planes may give valuable indications of potential danger.

It has been shown, that the classification method by Brewer and Marlow (1993), originally intended for an accurate 2D visualisation of a DEM, is suitable for the straightforward identification of planes/discontinuities from a DEM alone. Planes of the same discontinuity system can easily be identified over the whole wall. Their approximate slope and aspect is recognisable at a glance. Lastly, the method is very well transferable to other study sites.

2. To test some specified methods with respect to their suitability for characterising a partly glaciated alpine rock face. Those methods are (1) the six morphometric classes by Wood (1996), (2) the application of terrain roughness, and (3) of lidar reflectance intensity

(1) The six morphometric classes by Wood (1996) The application of Wood's method to a DEM of a steep, partially glaciated rock wall allows a quick overview of its morphometry, in particular relating to channel- and ridge-like features. Furthermore, smooth areas such as the snow/ice cover can be identified. Planar discontinuities, however, cannot be easily identified.

(2) Application of terrain roughness Terrain roughness is an important land-surface parameter and can be used for the extraction of specific elements used, for example, in studies related to wind analysis (Olaya, 2008). Vertical Ruggedness Measure (Sappington et al., 2007) is shown to be a suitable tool for the measurement of terrain roughness of a steep rock wall, since it is rather independent of slope. However, its use is recommended only at finer scales, because coarse-scale edges, such as rock ridges and steep fronts, are also seen as rough.

(3) Application of lidar reflectance intensity The use of lidar reflectance intensity may provide a possibility for the differentiation of snow/ice and bedrock. However, flight streaks are visible in the original data available for this study. Analyses of a small area might be possible, but for larger areas, the intensity data must first be corrected.

3. To consider and describe the influence of scale on all feature extraction methods that were evaluated within this study.

The influence of scale on DEM analysis is significant. Certain features can only be detected at a certain scale or range of scales. A multi-scale approach is imperative when extracting a feature from a DEM, in order to determine the suitable scale or scale range. Then, scale has to be adjusted to the dimension of the feature. Mostly, the minimum extent of the features gives the working scale, for instance in terms of cell size. It is therefore possible to identify a suitable scale for the extraction of a specific feature. By contrast, a most suitable scale cannot be assigned to a specific method when the target feature is not specified.

In some cases, however, the extraction of features is not dependent on scale (Shary et al., 2002). For instance, edges such as rock ridges or steep fronts were identified as being scale-independent, as they can be identified at all scales (or, more accurately, over a very large scale range).

The simultaneous visualisation of the influence of multiple scales on a land-surface parameter can give valuable insight into the effect of scale. Thus, in fuzzy set theory, each pixel is assigned the fraction of its membership to a class. With this approach, however, it is not evident in which classes the membership exists. Therefore, the binary numerical system was applied for classification, which permits at a glance the identification of the scale or scale range, over which a parameter value is above or below a given value (Fig. 5.8). Using this approach, the above mentioned independence of edges from scale was discovered.

7.2 Synthesis

Considering the totality of all applied methods, feature extraction on the available DEM shows the following:

1. In almost all applied methods, the land-surface parameter slope, which describes the rate of elevation change, plays a central role. Curvature, which describes the rate of slope change, was generally less important.

2. While satellite images and orthophotos are sufficient for the extraction of some specific features, laser scanning data is necessary in some cases since it provides geometrical information about the study site. It has been shown that the combination of image-based information and of lidar data is imperative for a successful extraction of a certain feature types, such as steep fronts.

3. The production process of the DEM that is used for analysis (for instance different grid interpolation methods) has a significant impact on the result of feature extraction.

4. Suitable thresholds for feature extraction are difficult to determine, because they depend on various factors. They differ with scale and also with the applied DEM processing methods (grid interpolation). They are very unstable, thus even small variations can lead to a quite different outcome. Therefore the thresholds may not be blindly transferred to other areas of interest but have to be visually examined.

5. A high-resolution DEM can be inappropriate for the extraction of coarser-scale features and may be first adapted to the dimension of the feature. Therefore, it is not always necessary to obtain or use high-detailed data.

Within the present work, only pixel-based methods were used for extraction because they are still very common and are convenient to apply. However, they usually do not lead to discrete area features.

In summary, the automated extraction of features from a DEM is useful or even necessary if the study area is very large or difficult to access. The latter particularly applies to the Monte Rosa east face.

7.3 Implications for future work

Changes in glacierised mountain regions will continue, affected by ongoing climate change (IPCC, 2007; Kääb et al., 2007). Slope instabilities in the Monte Rosa east face are very likely to continue to represent a critical hazard for this region. Therefore, remote sensing methods for the investigation of high-alpine walls should be further developed and improved. Among those methods, high-resolution airborne laser scanning provides valuable information about the geometry of the landscape, which permits feature extraction based on morphology.

Four feature types were specified for automated extraction because they are connected to the ongoing change processes within the rock wall. Although some of the determined extraction methods provide valuable results for the Monte Rosa east face, their transferability to other sites has yet to be tested. All the methods used here should be improved in order to obtain more accurate and more reliable results. Future enhancements could focus on the following aspects:

1. Almost all applied methods that were used to extract the four defined features, are dependent on thresholds. However, the use of thresholds reduces the reproducibility across implementations (Strobl, 2008) and the transferability across areas. Therefore, feature extraction methods should be considered that are less dependent on thresholds.

2. The reflectance intensity may provide a valuable source for an enhanced remote sensing analysis of the Monte Rosa east face. If the intensity values were corrected, e.g. according to Höfle and Pfeifer (2007), they could for instance be used for glacier surface segmentation (e.g. as been done by Höfle et al., 2007).

3. The applied multi-scale approach has been shown to be important for the extraction of specific features and should therefore be further considered and investigated. Pending points are (a) the behaviour of edges with scale, and (b) the influence of the grid interpolation method on feature extraction.

4. For the extraction of fine-scale features such as crevasses or even smaller objects, the quality of lidar production has to be improved such that laser streaks are not visible/recognisable at higher grid resolutions.

5. Terrain roughness is a complex land-surface parameter and can represent an important means for feature extraction. Since the evaluated calculation method according to Sappington et al. (2007) provides insufficient results relating edges at coarser scales,

a more accurate method should be found. The approach by (Sakude et al., 1998) may make it possible to improve these results.

6. It is likely that edges are recognised as rough at all scales, whatsoever roughness calculation method is applied. This assumption should be investigated, since it has a particular impact at coarser scales (cf. implication no. 5).

7. Instead of pixel-based, data-centric approaches, which were used in the present work, object-based approaches could be used to significantly improve feature extraction. When extracting area features, an object-based approach would lead to homogeneous and contiguous segments. Edge detection algorithms for the detection of line features could be optimised in order to better control the process. Object-based analysis could improve the transferability of the results and better incorporate the influence of scale.

8. All methodologies applied within the present work use a 2.5D approach, with each cell bearing only one height value. In order to detect overhanging rocks, which play a central role in slope stabilities, a 3D approach must be applied: either the original point cloud is used (without grid interpolation), or each cell can bear more than just one value.

9. The available lidar dataset covers the whole wall, which represents the area of interest for the hazard analyses. However, for certain DEM analyses (e.g. morphometric classes by Wood, 1996) the extent should not stop at the upper end of the wall, but should also include a small upper part of the other side of the mountain. This is also important for object-oriented approaches, which consider the topology and semantics of surface segments.

Apart from the mentioned enhancements regarding feature extraction methods, it will be desirable to automatically identify more features that are connected to the change processes in alpine flanks in the future. One possible feature type may be avalanche starting zones, which naturally present a high potential danger.

Bibliography

Baatz, M. and Schäpe, A. (2000). Multiresolution Segmentation — an optimization approach for high qualitiy multi-scale segmentation. In Strobl, J., Blaschke, T., and Griesebner, G., editors, *Angewandte Geographische Informationsverarbeitung XII*, Beiträge zum AGIT-Symposium Salzburg 2000, Karlsruhe. Wichmann.

Bearth, P. (1952). *Geologie und Petrographie des Monte Rosa*. Kümmerly & Frey, Bern.

Bellian, J., Kerans, C., and Jennette, D. (2005). Digital Outcrop Models: Applications of Terrestrial Scanning Lidar Technology in Stratigraphic Modeling. *Journal of sedimentary research*, 75(2):166–176.

Bolongaro-Crevenna, A., Torres-Rodríguez, V., Sorani, V., Frame, D., and Ortiz, M. A. (2005). Geomorphometric analysis for characterizing landforms in Morelos State, Mexico. *Geomorphology*, 67(3-4):407–422.

Brewer, C. A. and Marlow, K. A. (1993). Color representation of aspect and slope simultaneously. In *Proceedings of the International Symposium On Computer-Assisted Cartography*, Minneapolis, Minnesota.

Buckley, S., Vallet, J., Wheeler, W., and Braathen, A. (2008). Oblique helicopter-based Laser scanning for digital terrain modelling and visualisation of geological outcrops. In *ISPRS Congress*, Beijing.

Bue, B. and Stepinski, T. (2006). Automated classification of landforms on Mars. *Computers & Geosciences*, 32(5):604–614.

Burrough, P. A. (1986). *Principles of Geographical Information Systems for Land Resources Assessment*. Oxford University Press, USA.

Canny, J. (1986). A computational approach to edge detection. *IEEE Trans. Pattern Anal. Mach. Intell.*, 8(6):679–698.

Carleer, A., Debeir, O., and Wolff, E. (2005). Assessment of very high spatial resolution satellite image segmentations. *Photogrammetric Engineering and Remote Sensing*, 71:1285—1294.

Chorowicz, J., Parrot, J., Taud, H., Hakdaoui, M., Rudant, J. P., and Rouis, T. (1995).

Automated pattern-recognition of geomorphic features from DEMs and satellite images. *Z. Geomorph. N.F.*, 101:69–84.

Cross, A. (1988). Detection of circular geological features using the Hough transform. *International Journal of Remote Sensing*, 9(9):1519—1528.

Derron, M., Jaboyedoff, M., and Blikra, L. H. (2005). Preliminary assessment of rockslide and rockfall hazards using a DEM (Oppstadhornet, Norway). *Nat. Hazards Earth Syst. Sci.*, 5(2):285–292.

Dikau, R. (1989). The application of a digital relief model to landform analysis in geomorphology. In Raper, J., editor, *Three dimensional applications in geographic information systems*, pages 51–77. Taylor & Franics, London, New York, Philadelphia.

Dragut, L. and Blaschke, T. (2006). Automated classification of landform elements using object-based image analysis. *Geomorphology*, 81(3-4):330–344.

Elewa, A. M. (2004). *Morphometrics: Applications in Biology and Paleontology*. Springer, 1 edition.

ESRI (2006). *ArcView 9.2*. ESRI, Redlands, CA.

Evans, I. (1972). General geomorphometry, derivatives of altitude, and descriptive statistics. In Chorley, R., editor, *Spatial Analysis in Geomorphology*, pages 17–90. Methuen, London.

Evans, I. (1979). *An integrated system of terrain analysis and slope mapping*. Statistical characterization of altitude matrices by computer – report 6. University of Durham, Department of Geography, Durham.

Evans, I. (1987). A new approach to drumlin morphometry. In Menzies, J. and Rose, J., editors, *Drumlin Symposium*, pages 119—130. AA Balkema Publishers, Balkema, Rotterdam.

Evans, I., Hengl, T., and Gorsevski, P. (2008). Applications in Geomorphology. In Hengl, T. and Reuter, H., editors, *Geomorphometry: Concepts, Software, Applications*, volume 33 of *Developments in Soil Science*, pages 497–525. Elsevier.

Fischer, L. (2004). *Monte Rosa Ostwand — Geologie, Vergletscherung, Permafrost und Sturzereignisse in einer hochalpinen Steilwand*. Unpublished diploma thesis, ETH Zürich.

Fischer, L. (2006). Monte Rosa Ostwand — Geologie, Vergletscherung, Permafrost und Sturzereignisse in einer hochalpinen Steilwand. *Bull. angew. Geol.*, 11(1):65–78.

Fischer, L. (in prep.). *Slope instabilities in perennially frozen and glacierised rock walls: analysis and modeling*. Ph.D. thesis, University of Zurich.

Fischer, L., Eisenbeiss, H., Kääb, A., Huggel, C., and Haeberli, W. (submitted). Detecting topographic changes in steep high-mountain flanks using combined repeat airborne LiDAR and aerial optical imagery — a case study on climate-induced hazards at Monte Rosa east face, Italian Alps. *Journal of Geophysical research*.

Fischer, L., Kääb, A., Huggel, C., and Noetzli, J. (2006). Geology, glacier retreat and permafrost degradation as controlling factors of slope instabilities in a high-mountain rock wall: the Monte Rosa east face. *Nat. Hazards Earth Syst. Sci.*, 6(5):761–772.

Fisher, P., Wood, J., and Cheng, T. (2004). Where is Helvellyn? Fuzziness of multi-scale landscape morphometry. *Transactions of the Institute of British Geographers*, 29:106—128.

Garbrecht, J. and Martz, L. (1994). Grid size dependency of parameters from digital elevation models. *Computers & Geosciences*, 20(1):85–87.

Gerrard, A. and Robinson, D. (1971). Variability in slope measurements. A discussion of the effect of different recording intervals and micro-relief in slope studies. *Trans. Inst. Br. Geographers*, 54:45–54.

Haeberli, W., Kääb, A., Paul, F., Chiarle, M., Mortara, G., Mazza, A., Deline, P., and Richardson, S. (2002). A surge-type movement at Ghiacciaio del Belvedere and a developing slope instability in the east face of Monte Rosa, Macugnaga, Italian Alps. *Norwegian Journal of Geography*, 56:104—111.

Hengl, T. (2006). Finding the right pixel size. *Computers & Geosciences*, 32(9):1283–1298.

Hengl, T. and Evans, I. (2008). Mathematical and Digital Models of the Land Surface. In Hengl, T. and Reuter, H., editors, *Geomorphometry: Concepts, Software, Applications*, volume 33 of *Developments in Soil Science*, pages 31–63. Elsevier.

Hengl, T. and MacMillan, R. (2008). Geomorphometry — A Key to Landscape Mapping and Modelling. In Hengl, T. and Reuter, H., editors, *Geomorphometry: Concepts, Software, Applications*, volume 33 of *Developments in Soil Science*, pages 433–460. Elsevier.

Hengl, T. and Reuter, H. (2008). *Geomorphometry: Concepts, Software, Applications*. Elsevier.

Hobson, R. (1972). Surface roughness in topography: quantitative approach. In Chorley, R., editor, *Spatial analysis in geomorphology*, pages 221–245. Methuen, London.

Höfle, B., Geist, T., Rutzinger, M., and Pfeifer, N. (2007). Glacier surface segmentation using airborne laser scanning point cloud and intensity data. *IAPRS*, XXXVI(Part 3, W52).

Höfle, B. and Pfeifer, N. (2007). Correction of laser scanning intensity data: Data and model-driven approaches. *ISPRS Journal of Photogrammetry and Remote Sensing*, 62(6):415–433.

IPCC (2007). Climate Change 2007: The Physical Science Basis. Contribution of Working Group I to the Fourth Assessment Report of the Intergovernmental Panel on Climate Change. Technical report, Cambridge University Press, Cambridge, United Kingdom and New York.

Jaboyedoff, M., Baillifard, F., Couture, R., Locat, J., and Locat, P. (2004). New insight of geomorphology and landslide prone area detection using DEM. In Lacerda, W., Ehrlich, M., Fontoura, A., and Sayo, A., editors, *Landslides Evaluation and stabilization*, page 199–205. Balkema.

Kääb, A. (2008). Remote sensing of permafrost-related problems and hazards. *Permafrost and Periglacial Processes*, 19(2):107–136.

Kääb, A., Chiarle, M., Raup, B., and Schneider, C. (2007). Climate change impacts on mountain glaciers and permafrost. *Global and Planetary Change*, 56(1-2):vii–ix.

Kääb, A., Huggel, C., Barbero, S., Chiarle, M., Cordola, M., Epifani, F., Haeberli, W., Mortara, G., Semino, P., Tamburini, A., and Viazzo, G. (2004). Glacier hazards at Belvedere Glacier and the Monte Rosa east face, Italian Alps: processes and mitigation. In *Internationales Symposium Interpraevent*, pages 67–78, Riva/Trient.

Kodde, M., Pfeifer, N., Gorte, B., Geist, T., and Höfle, B. (2007). Automatic glacier surface analysis from airborne laser scanning. *IAPRS*, 36(Part 3, W52).

Kohavi, R. and Provost, F. (1998). Glossary of Terms. *Machine Learning*, 30(2):271–274.

Kubat, M., Holte, R. C., Matwin, S., Kohavi, R., and Provost, F. (1998). Machine learning for the detection of oil spills in satellite radar images. *Machine Learning*, 30:195—215.

Lee, S., Yu, T., Wang, C., and Peng, W. (2007). Automatic Geological Lineaments Extraction from Digital Elevation Model of Airborne LiDAR. *Geophysical Research Abstracts*, 9.

Li-chun, S. (2002). *Analysis of Laser Scanner Data by Means of Digital Image Processing Techniques*. PhD dissertation, Berlin Technical University.

Longley, P., Goodchild, M. F., Maguire, D., and Rhind, D. (2005). *Geographic Information Systems and Science*. Wiley, New York, 2 edition.

MacMillan, R. and Shary, P. (2008). Landforms and Landform Elements in Geomorphometry. In Hengl, T. and Reuter, H., editors, *Geomorphometry: Concepts, Software, Applications*, volume 33 of *Developments in Soil Science*, pages 227–254. Elsevier.

Mark, D. and Smith, B. (2004). A science of topography: from qualitative ontology to digital representations. In Bishop, M. and Shroder, J., editors, *Geographic Information Science and Mountain Geomorphology*, pages 75—97. Springer-Praxix, Chichester, England.

Mark, D. M. (1975). Geomorphometric Parameters: A Review and Evaluation. *Geografiska Annaler. Series A, Physical Geography*, 57(3/4):165–177. ArticleType: primary_article / Full publication date: 1975 / Copyright © 1975 Swedish Society for Anthropology and Geography.

Mason, D. C., Scott, T. R., and Wang, H. (2006). Extraction of tidal channel networks from airborne scanning laser altimetry. *ISPRS Journal of Photogrammetry and Remote Sensing*, 61(2):67–83.

Miliaresis, G. and Kokkas, N. (2007). Segmentation and object-based classification for the extraction of the building class from LIDAR DEMs. *Comput. Geosci.*, 33(8):1076–1087.

Miliaresis, G. C. and Argialas, D. P. (1999). Segmentation of physiographic features from the global digital elevation model/GTOPO30. *Comput. Geosci.*, 25(7):715–728.

Nelson, A., Reuter, H., and Gessler, P. (2008). DEM Production Methods and Sources. In Hengl, T. and Reuter, H., editors, *Geomorphometry: Concepts, Software, Applications*, volume 33 of *Developments in Soil Science*, pages 65–85. Elsevier.

Olaya, V. (2008). Basic Land-Surface Parameters. In Hengl, T. and Reuter, H., editors, *Geomorphometry: Concepts, Software, Applications*, volume 33 of *Developments in Soil Science*, pages 141–169. Elsevier.

Pike, R., Evans, I., and Hengl, T. (2008). Geomorphometry: A Brief Guide. In Hengl, T. and Reuter, H., editors, *Geomorphometry: Concepts, Software, Applications*, volume 33 of *Developments in Soil Science*, pages 3–30. Elsevier.

Pike, R. J. (2000). Geomorphometry — diversity in quantitative surface analysis. *Progress in Physical Geography*, 24(1):1–20.

Pitas, I. (1993). *Digital Image Processing Algorithms*. Prentice Hall.

Post, A. and Lachapelle, E. R. (1971). *Glacier Ice*. University of Toronto Press.

Pralong, A. and Funk, M. (2006). On the instability of avalanching glaciers. *Journal of Glaciology*, 52:31–48(18).

R Development Core Team (2008). *R: A Language and Environment for Statistical Computing*. R Foundation for Statistical Computing, Vienna, Austria.

Rabatel, A., Deline, P., Jaillet, S., and Ravanel, L. (2008). Rock falls in high-alpine rock walls quantified by terrestrial lidar measurements: A case study in the Mont Blanc area. *Geophys. Res. Lett.*, 35.

Ravanel, L., Deline, P., Jaillet, S., and Rabatel, A. (2008). Quantifying rock falls/avalanches in steep high-alpine rock walls: three years of laserscanning in the Mont Blanc massif. *Geophysical Research Abstracts*, 10.

Russ, J. C. (1999). *The Image Processing Handbook*. CRC.

Sakude, M. T., Schiavone, G. A., Morelos-Borja, H., Martin, G., Cortes, A., and Sisti, A. F. (1998). Recent advances on terrain database correlation testing. In *Enabling Technology for Simulation Science II*, volume 3369, pages 364–376, Orlando, FL, USA. SPIE.

Sappington, J. M. (2008). *Vector Ruggedness Measure*. Retrieved 12 June 2009 from http://arcscripts.esri.com/details.asp?dbid=15423.

Sappington, J. M., Longshore, K. M., and Thompson, D. B. (2007). Quantifying Landscape Ruggedness for Animal Habitat Analysis: A Case Study Using Bighorn Sheep in the Mojave Desert. *Journal of Wildlife Management*, 71(5):1419–1426.

Schmidt, J. and Andrew, R. (2005). Multi-scale landform characterization. *Area*, 37(3):341–350.

Serra, J. (1982). *Image analysis and mathematical morphology*. Academic Press.

Sharp, R. P. (1988). *Living Ice*. Cambridge University Press, Cambridge.

Shary, P., Sharaya, L., and Mitusov, A. (2002). Fundamental quantitative methods of land surface analysis. *Geoderma*, 107:1—32.

Skaloud, J., Vallet, J., Keller, K., Veyssière, G., and Kölbl, O. (2005). HELIMAP: Rapid Large Scale Mapping Using Handheld LiDAR/CCD/GPS/INS Sensors on Helicopters. In *Proceedings of the ION GNSS Conference*, Long Beach, California.

Smith, M. P., Zhu, A., Burt, J. E., and Stiles, C. (2006). The effects of DEM resolution and neighborhood size on digital soil survey. *Geoderma*, 137(1-2):58–69.

Smith, S. (2005). Topographic mapping. In Grundwald, S., editor, *Environmental Soil–Landscape Modelling: Geographic Information Tecnologies and Pedometrics*, volume 1, pages 155—182. CRC Press, New York.

Srivastava, A. and Stroeve, J. (2003). Onboard Detection of Snow, Ice, Clouds and Other Geophysical Processes Using Kernel Methods. In *Proceedings of the ICML 2003 Workshop on Machine Learning Technologies for Autonomous Space Sciences*, Washington, DC, USA.

Straumann, R. K. and Purves, R. S. (2008). Delineation of Valleys and Valley Floors. In *Proceedings of the 5th international conference on Geographic Information Science*, pages 320–336, Park City, UT, USA. Springer-Verlag.

Strobl, J. (2008). Segmentation-based Terrain Classification. In Zhou, Q., Lees, B., and an Tang, G., editors, *Advances in Digital Terrain Analysis*, pages 125–139. Springer, Berlin, Heidelberg.

The MathWorks (2007). *MATLAB R2007a*. The MathWorks, Natick, MA.

Tribe, A. (1990). Towards the automated recognition of landforms (valley heads) from digital elevation models. In *Proceedings of the 4th Intern. Symposium on Spatial Data Handling*, pages 45–52, Zürich.

Vallet, J. (2007). GPS/IMU and LiDAR integration to aerial photogrammetry: Development and practical experiences with Helimap System®. In *Vorträge Dreiländertagung 27. Wissenschaftlich-Technische Jahrestagung der DGPF*, Muttenz.

Vallet, J. and Skaloud, J. (2004). Development and Experiences with A Fully-Digital Handheld Mapping System Operated From A Helicopter. *The International Archives of the Photogrammetry, Remote Sensing and Spatial Information Sciences*, XXXV(Part B, Commission 5).

Venkataraman, G., Singh, G., and Kumar, V. (2008). Snow cover area monitoring using multi-temporal TerraSAR-X data. In *3. TerraSAR-X Science Team Meeting*, Oberpfaffenhofen.

Wang, L., Sousa, W., and Gong, P. (2004). Integration of object-based and pixel-based classification for mapping mangroves with IKONOS imagery. *International Journal of Remote Sensing*, 25(24):5655.

Weibel, R. and Heller, M. (1991). Digital Terrain Modeling. In Maguire, D., Goodchild, M., and Rhind, D., editors, *Geographical Information Systems: Principles and Applications*, pages 269–297. Longman, London.

Wood, J. (1996). *The Geomorphological Characterisation of Digital Elevation Models*. PhD thesis, University of Leicester.

Wood, J. (2007). *LandSerf 2.3*. J.D. Wood, City University, London, UK.

Xu, J., Wan, Y., Zhang, X., Zhang, L., and Chen, X. (2006). A method of edge detection based on improved canny algorithm for the lidar depth image. In *Geoinformatics 2006: Remotely Sensed Data and Information*, volume 6419. SPIE.

Zhou, M., Xia, B., Su, G., Tang, L., and Li, C. (2008). Study on the target feature extraction from lidar point clouds. In *Proceedings of Commission III*, Beijing.